Development of Capsaicin-based Nanoemulsions: Structural Characterisation and in Vitro Evaluation

Junyi Xu

Submitted in accordance with the requirements for the degree of

Master of Science by Research

in

Food science

The University of Leeds

School of Food Science & Nutrition

February, 2021

The candidate confirms that the work submitted is her own and that appropriate credit has been given where reference has been made to the work of others.

Acknowledgements

The present work contained in this dissertation was carried out at the University of Leeds in the School of Food Science & Nutrition within the Research Group of Biopolymers led by Professor Francisco M. Goycoolea. This research project was carried out from October 2019 to February 2021.

I would like to thank all the people that have made contributions to this work in one way or another. Without your kind support, this work could not have been achieved under the circumstances faced through the challenging times caused by Covid-19.

Firstly, I would like to express my sincere gratitude to my supervisor Prof. Francisco Goycoolea Valencia for his precious guidance and inspiration through this project which allowed me to get a better insight into this.

I would also thank Dr. Yadira Gonzalez Espinosa for her kind help throughout my degree. Her hard work, reliability, patience and other good manners have greatly influenced me.

Many thanks to Dr. Elena Simone for her professional advice and useful suggestions at the final stage of this project.

Thanks to Dr. Mattias Kaiser from Germany for his time and kind help to work out the protocols of impedance measurements.

Many thanks to Mr. Martin Fuller from the Astbury Centre at the Faculty of Biological Sciences of the University of Leeds for his assistance with the TEM images.

I would also like to acknowledge the technical team at the School of Food Science and Nutrition, especially to Miles Ratcliffe, Sara Viney, Joanna Sier and Neil Rigby, for their skilful training and assistance.

Thanks to all the team members of my research group for many great moments together. I will miss you.

And last but not least, I am very grateful to my parents and my dear husband, Guohao Du. Their unconditional love and support have always encouraged me to be the best.

Abstract

Background and objective: Capsaicin, the bioactive component in hot chilli peppers, has been demonstrated to induce reversible opening of epithelial cellular tight junctions. The aim of this research project was to study the formation of capsaicin nanoparticles and assess their potential as a Pickering emulsifier in o/w systems formed by the solvent displacement method. This microstructural approach could attenuate the drawbacks (e.g. pungency, low water solubility and cytotoxicity at high concentration) of capsaicin while at the same time exert its effect as a potential drug delivery enhancer through paracellular pathway.

Methods: To synthesize highly monodispersed capsaicin nanoparticles, the equilibrium and the solubility behaviour of capsaicin were studied in the ternary system: capsaicin-water-ethanol to identify the ouzo region. Then, a capsaicin-based nanoemulsion was formulated and characterised. The microstructure of the system has also been evaluated. Finally, assessments of cell cytotoxicity and permeability were carried out by monitoring impedance measurements in MDCK II cell monolayers.

Results: Highly monodispersed capsaicin nanoparticles were formed in the ouzo region. Stable capsaicin-based nanoemulsions were also developed by the solvent displacement method while harnessing the ouzo effect. However, TEM images seemed to suggest that the mechanism of stabilisation of nanoemulsion might be different to the Pickering stabilization. *In vitro* cytotoxicity and permeability studies revealed that the nanoemulsion attenuated the cytotoxic effect of capsaicin on MDCK II cells and modulated the reversible tight junctions opening.

Conclusions: This study provides new insights into the development of o/w emulsions with capsaicin and may lead to novel oral drug delivery applications.

Table of Contents

List of Tables

List of Figures

Chapter 1
Introduction

Drugs can be delivered into the body by various routes as depicted in Figure 1.1. Compared to other routes of administration (ROA), oral drug delivery has been used most frequently due to its simplicity, sustained delivery, convenience and patient compliance (Homayun et al., 2019). However, this administration route is complex due to the absorption of drugs occurring in the gastrointestinal tract (GI tract). Multiple levels of barriers must be overcome before drugs reach their sites of action, which leads to low bioavailability of some drugs.

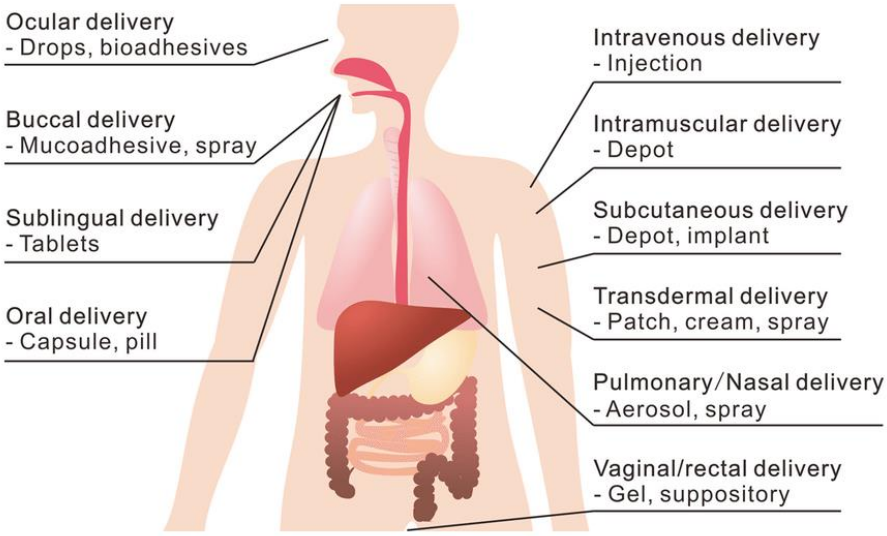

Figure 1.1 Routes of drug administration (National Pain Centers, 2019).

Barriers for poor bioavailability of oral drug delivery are as follows: (a) the mucus layers and the epithelium of intestinal mucosa form physiological barriers for the passage of drugs; (b) biochemical barriers consisting of metabolizing enzymes and efflux systems that can degrade drugs, are obstacles for drug delivery as well (Kiptoo et al., 2016); (c) the physicochemical properties of a drug determining its solubility and membrane permeability. According to biopharmaceutical classification system (Table 1.1), low water solubility or low membrane permeability of drugs in class II and

class III can be chemical barriers to limit their oral bioavailability (Svenson, 2004).

Table 1.1 Drug classification by biopharmaceutical classification system (Amidon et al., 1995).

	High permeability	Poor permeability
High solubility	Class I	Class III
Poor solubility	Class II	Class IV

Thus, there is a need to prevent drug degradation and enhance drug absorption through oral delivery. Nanocarriers are investigated extensively to provide an alternative solution to administer active pharmaceutical ingredients (API) with improved bioavailability and therapeutic effect (Sharma et al., 2016). Due to their high surface area to volume ratio, this kind of drug delivery systems has the ability to enhance solubility and cellular contact, resulting in higher bioavailability in the GI tract (Zhang et al., 2013). Besides, they can also provide additional benefits such as improved pharmacokinetics and biodistribution, site-specific delivery, controlled release and attenuated dose-related toxicities (Din et al., 2017). Nanocarrier systems like liposomes, micelles, emulsions, nanoparticles and capsules are widely used for drug delivery. The formulations and applications of these carriers have been broadly reviewed in many papers (Zhang et al., 2013; Svenson, 2004; Sharma et al., 2016) and their structures are shown in Figure 1.2.

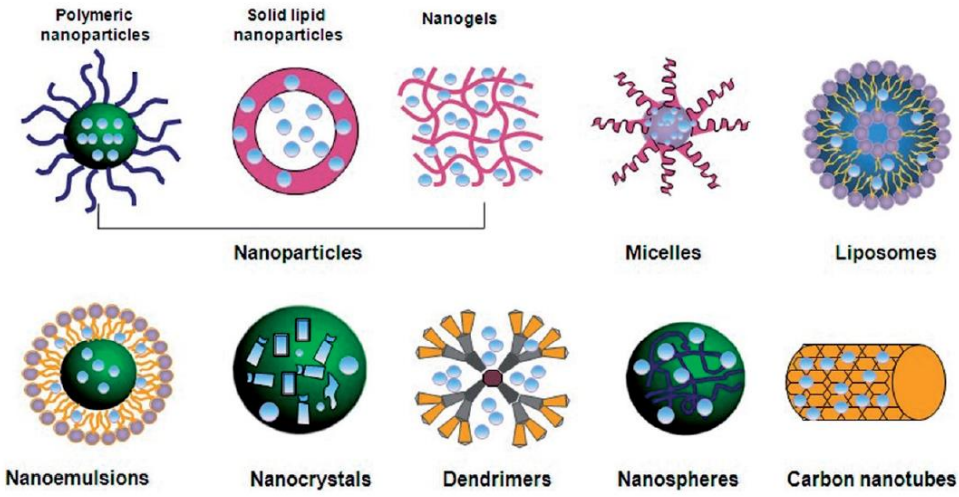

Figure 1.2 Structures of different nanocarrier systems (Zhang et al., 2013).

Compared to other nanocarriers, nanoemulsions (NEs) are easier to prepare and have a higher drug loading capacity (Patel et al., 2017). NEs have been widely used as a vehicle for poorly soluble drugs since they can enhance the bioavailability by protecting the encapsulated API and enhancing its solubility. Besides, they can also mask the possible unpleasant taste or texture, making them more acceptable for oral delivery (Lachman et al., 1986). Generally, they are colloidal dispersions of two immiscible liquids, oil and water, with/without surfactants, forming oil-in-water (o/w) or water-in-oil (w/o) systems with the size of droplets less than 200 nm (Shaker et al., 2019). Due to the positive Gibbs free energy required to increase the water/oil interfacial area, nanoemulsions have a higher free energy than the phase separated state. Thus, they are thermodynamically unstable. However, nanoemulsions are kinetically stable due to their extremely small particle size. Those particles are involved into Brownian motion, thereby preventing gravitational separation (creaming/sedimentation) or droplet aggregation (coalescence/flocculation) (McClements, 2021). The Ostwald ripening, which describes the growth of large droplets at the expense of smaller ones, is the main issue for their stability (Anton and Vandamme, 2011). This mass transport process is typically driven by differences in chemical potentials for the solutes in droplets of different sizes. Those smaller droplets have higher chemical potentials and greater solubility than larger droplets, leading to molecular diffusion from smaller droplets to larger droplets because of the concentration gradient. Using a compound less soluble in the continuous phase as the dispersed phase can decrease the rate of Ostwald ripening (Koroleva and Yurtov, 2012).

Recent progress has shown that Pickering emulsions, stabilised by solid particles, have the ability to slow down Ostwald ripening and display higher stability (Whitby and Wanless, 2016). This kind of emulsions can also avoid the use of traditional surfactants, leading to higher safety for *In vivo* usage. These systems have gained substantial traction given their applications in various areas such as foods, pharmaceuticals and cosmetics.

Capsaicin is a natural alkaloid occurring in hot chilli peppers of Capsicum family and it is responsible for the pungency sensation. As one of the predominant capsaicinoids, it exerts various biological properties such as chronic pain relieving, body temperature regulation and obesity reduction, among others. Previous researches have demonstrated that capsaicin treatment induced reversible tight junction opening. Though the underlying mechanisms are under extensive investigation and not fully understood yet, capsaicin has been suggested as a new type of paracellular permeability

enhancer to enhance the delivery of hydrophilic macromolecular drugs across biological barriers.

The overall goal of this project was to assess the formation of a novel capsaicin-loaded NE system by the solvent displacement method. Highly monodispersed and stable capsaicin nanoparticles were obtained within the ouzo region of a ternary phase diagram (ethanol-water-capsaicin). We hypothesized that the capsaicin nanoparticles generated would be adsorbed simultaneously at the oil/water interface to form a Pickering emulsion favoured by the nanosize of the particles created. The advantage of this approach would be low energy input, absence of surfactant and simplicity for its formation at laboratory scale. NEs in this case, were produced only in one step due to the rapid diffusion of the organic phase into the aqueous phase and the supersaturation of hydrophobic solutes.

Chapter 2
Literature Review

2.1 Introduction

In this chapter, a broad review of relevant literature about capsaicin and capsaicinoids, Pickering emulsions, solvent displacement and the ouzo effect, cellular tight junctions is included to provide background knowledge and set the motivation behind this work and fundamentals for its development.

2.2 Capsaicin and capsaicinoids

Capsaicinoids are a group of non-volatile alkaloids present in Capsicum. They are hydrophobic, colourless, odourless, crystalline and responsible for pungent and hot sensations of chilli peppers. To date, there are about 25 different natural capsaicinoids identified (Valim et al., 2019). Capsaicin and dihydrocapsaicin, comprising about 90% of capsaicinoids in chilli peppers, are the two major ones. Other capsaicinoids include homocapsaicin, homodihydrocapsaicin, norcapsaicin and nordihydrocapsaicin, among others.

The content of capsaicinoids in chillies directly affects their pungency which can be either assessed precisely by analytical methods such as high-performance liquid chromatography (HPLC) with UV or fluorescence detection, or roughly estimated by sensory determinations and the Scoville scale. The Scoville heat units (SHU) is the number of times the chilli extract is diluted until no detectable heat is perceived through the sensory test (Scoville, 1912). The sweet bell pepper for example, is zero SHU while the habanero pepper, one of the hottest chillies, is 200,000–300,000 SHU. Pure capsaicin and dihydrocapsaicin are 16 million SHU, nearly twice the pungency compared to other capsaicinoids (Juturu, 2016).

2.2.1 Chemical structure

Capsaicinoids are from the vanilloid family and they share a similar structure comprising a vanillyl group and C9-C11 branched chain fatty acid with an amide group (Hayman and Kam, 2008). Figure 2.1 shows the chemical

structures assigned to the six main capsaicinoids. They are different in the length of the branched chain fatty acids or the number of unsaturation.

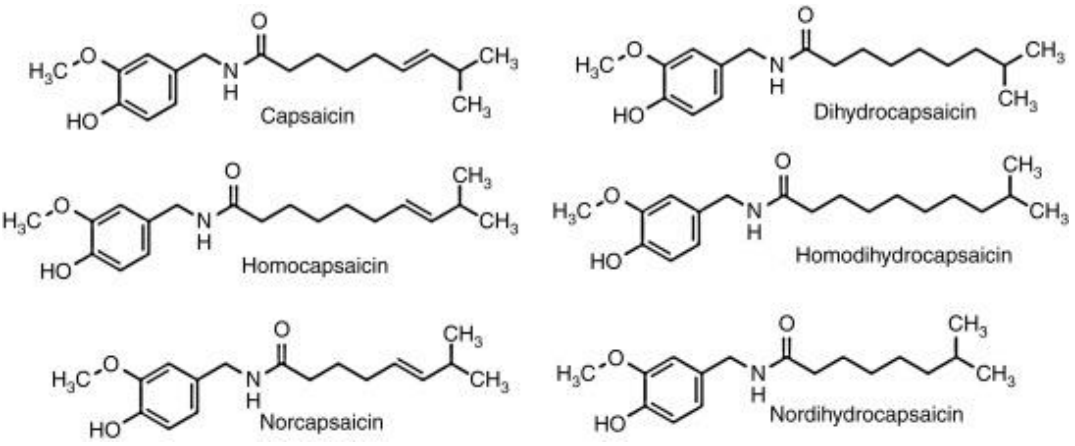

Figure 2.1 Chemical structures of six main capsaicinoids (Kulkarni et al., 2017).

2.2.2 Functional properties and biological effects of capsaicin

Capsaicinoids, especially capsaicin, play an important role in food and pharmaceutical industries. It is essential to understand its biological and physiological activities. Many articles have reviewed the health benefits of capsaicin such as pain management, anti-cancer, anti-obesity and cardio-protective effect.

It is well known that the burn and pain sensation caused by hot chilli peppers is mainly due to capsaicin, which is an agonist that can bind to the transient receptor potential vanilloid 1 (TRPV1). TRPV1 is also a receptor for other physical and chemical stimulus such as zingerone, noxious heat (> 43°C), low pH, voltage and lipids, leading to pain sensations (Jara-Oseguera et al., 2008; Tominaga and Tominaga, 2005). This phenomenon is called nociception. TRPV1, a nonselective cation channel with high permeability to Ca^{2+}, can be found in many sensory nerve fibres as well as non-neuronal tissues such as kidney, bladder (Jara-Oseguera et al., 2008; Du et al., 2019). As Figure 2.2 shows, TRPV1 consists of six transmembrane domains, a pore-forming hydrophobic region located between the fifth and sixth transmembrane domains and intracellular N and C terminal tails. Since capsaicin is hydrophobic, it can cross the cell membrane and interact with the cytoplasmic domain of the third and fourth transmembrane proteins on TRPV1. The binding is via hydrogen bonding and Van der Waals interaction with a “hydrophobic tail up, vanillyl head down” configuration (Du et al., 2019; Yang and Zheng, 2017; Fattori et al., 2016). Then TRPV1 is activated via

phosphorylation by protein kinases, leading to calcium influx and the release of neuropeptides (substance P) (Lu et al., 2020). While the dephosphorylation of the receptor and depletion of substance P by an intracellular Ca^{2+}-dependent mechanism, result in a decrease in receptor sensitivity (Smutzer and Devassy, 2016; Kaiser et al., 2017). Therefore, the repeated exposure of TRPV1 to capsaicin can lead to the desensitization of this receptor, allowing the utilisation of capsaicin and its analogues topically to relieve muscle and joint pains (Fattori et al., 2016).

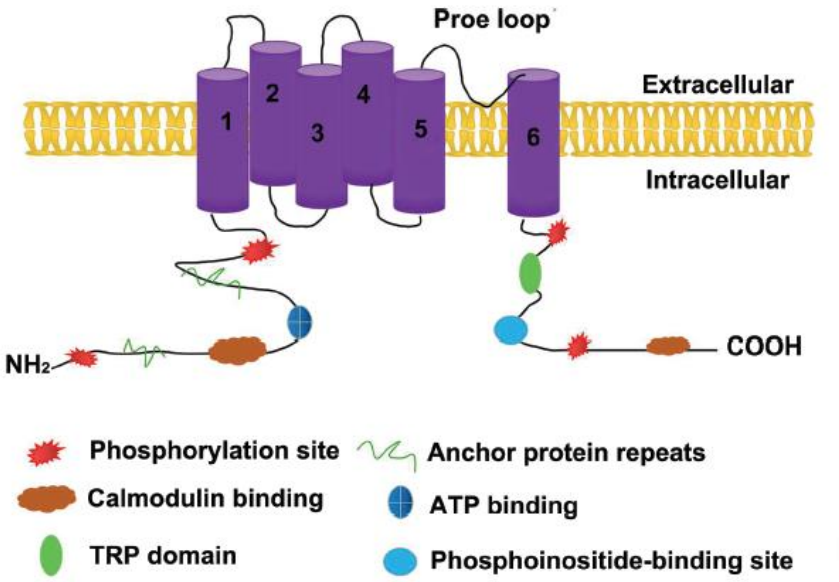

Figure 2.2 Schematic diagram illustrating the structure of TRPV1 channel (Du et al., 2019).

In addition, capsaicin may have the potential to improve cardiovascular health due to its blood pressure regulation activity by enhancing the release of neuropeptide calcitonin gene-related peptide (CGRP) through TRPV1 activation (Peng and Li, 2010). In this case, other mechanisms have also been discovered, such as a decrease in lipid storage, attenuating atherosclerosis (Ma et al., 2011), reducing platelet aggregation (Almaghrabi et al., 2016), among others.

Moreover, capsaicin has a beneficial role in weight loss and obesity reduction where it has been shown that satiety and fullness can be enhanced by addition of capsaicin to the diet (Westerterp-Plantenga et al., 2004). Furthermore, many studies have reported that capsaicin could target multiple signalling pathways and modulate gene expression involved in the proliferation,

apoptosis and metastasis of tumour or cancer cells, suggesting the anti-cancer potential of capsaicin against various human cancers (Clark and Lee, 2016; Cho et al., 2017).

Recently, many experiments have demonstrated that capsaicin induced reversible epithelial cells tight junctions opening (Kaiser et al., 2015; Salama et al., 2006). Reversible opening of tight junctions would benefit the therapeutic effect since it avoids the entry of metabolic waste as well as the leakage of important proteins and nutrients for too long time. Therefore, it offers an opportunity to mediate cell permeability and enhance the absorption of hydrophilic macromolecular drugs through the paracellular pathway. Further explanation to this is provided within section 2.3.3.

Though capsaicin has a variety of pharmacological properties, clinical applications have been limited due to its strong pungency, low water solubility and cytotoxicity at higher doses. Delivery systems such as liposomes, micelles, nanoemulsions have been developed to encapsulate capsaicin in order to enhance the oral bioavailability as well as to relieve the irritation in the gastrointestinal mucosa (Lu et al., 2020). Other studies have also led to the discovery of non-pungent analogues such as capsiate, dihydrocapsiate (Kobata et al., 1998) and palvanil (Luongo et al., 2012). Also, non-pungent glycosylated capsaicin derivatives have been obtained by biotransformation methods using plant cultured cells (Kometani et al., 1993).

2.2.3 Capsaicin as cell tight junctions modulator

Many studies have been conducted to elucidate the mode of action behind the effect of capsaicin on cell permeability. Among these studies, human colon adenocarcinoma (Caco-2) and Madin-Darby Canine Kidney (MDCK) cell monolayers are most intensively used as *in vitro* models to evaluate cell permeability, since they form strong tight junctions and are easy and rapid to cultivate (Volpe, 2011).

A research group in Japan uncovered the mechanism underlying the tight junctions opening action of capsaicin in intestinal Caco-2 cells. It was demonstrated that cell permeability was increased with a high concentration of capsaicin from 200 to 500 µM after 45 min. By monitoring intracellular Ca^{2+} and Lactate Dehydrogenase (LDH) activity, they confirmed that this level of capsaicin concentration was safe to the cell monolayer (Isoda et al., 2001). In a later study, they found that cell permeability, assessed by TEER (transepithelial/transendothelial electrical resistance), can be completely

recovered with 100 μM capsaicin treatment as Figure 2.3a showed (Han et al., 2005). But they did not test the reversible effect of capsaicin treatment at higher concentrations.

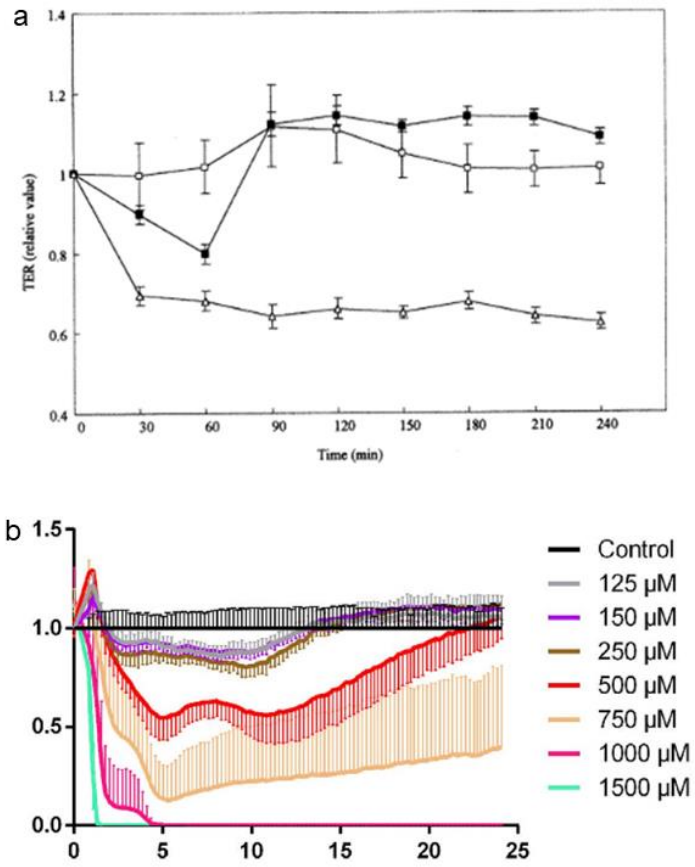

Figure 2.3 Effects of free capsaicin on TEER along with time. (a) Relative TEER in Caco-2 cells, capsaicin concentrations were 0 μM (open boxes), 100 μM (filled boxes), and 1 mM (open triangles) (Han et al., 2005). (b) Normalized TEER in MDCK-C7 cells (Kaiser et al., 2015b).

As for the mechanism, the binding between capsaicin and its vanilloid receptor was initially suggested (Isoda et al., 2001). After that, they revealed that the decrease in the amount of filamentous actin (F-actin) and heat shock protein (HSP47) expression happened during capsaicin-induced tight junctions opening (Han et al., 2002). But for the reversible effect, they showed that ribosomal protein P2 was expressed significantly leading to the activation of elongation factor 2, which stabilized F-actin (Han et al., 2005). Cofilin is one of the actin-depolymerizing factors and activation of cofilin was found to correlate with Ca^{2+} influx induced by capsaicin (Nagumo et al., 2007). Further, they suggested that relocation of F-actin, ZO-1 and Claudin-1 happened along with actin alteration after capsaicin treatment. These results showed that

cofilin is the key factor in tight junctions opening in epithelial cells (Nagumo et al., 2008).

Studies in MDCK-C7 cells showed that TEER increased and peaked during the first 20 min, and then decreased in a capsaicin dose-dependent manner. After 24 h, the TEER recovered to the original values except when the concentration of capsaicin exceeded 500 μM (Figure 2.3b). An MTT (3-(4,5-dimethylthiazol-2-yl)-2,5-diphenyltetrazolium bromide) assay indicated that capsaicin exhibited cytotoxicity when the concentration was higher than 300 μM. However, capsaicin-loaded nano-formulations such as nanoemulsions and nanocapsules can substantially attenuate the decrease of TEER, which allows the application of higher concentrations of capsaicin (Kaiser et al., 2015).

They also investigated the effect of capsaicin derivatives on MDCK-C7 cells and found that less lipophilic vanilloids showed a rapid effect on TJ opening after administration. In this case and opposite to Caco-2 cells, the TRPV1 receptor is not necessarily required to induce this effect in MDCK-C7 cells since Ca^{2+} influx was not observed (Kaiser et al., 2016b).

Similarly as in Caco-2 cells, dephosphorylation of cofilin and depolymerization of actin were also found along with tight junctions opening in MDCK II cells. Even more, the depolymerization of actin mainly occurred at bicellular tight junctions and there was a shift in the location of F-actin to the apical side as illustrated in Figure 2.4. This kind of actin alteration was found to be capsaicin-specific. Besides, they did not observe any change in the location of protein with the treatment of capsaicin, but the amount of occludin decreased significantly (Shiobara et al., 2013).

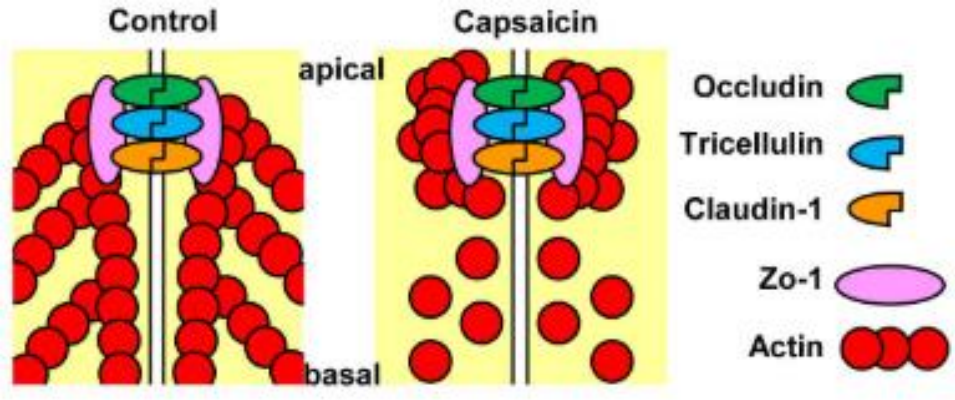

Figure 2.4 Effects of capsaicin on the actin depolymerization and distribution of F-actin (Shiobara et al., 2013).

In MDCK II cells, Ca^{2+} influx was found to be relevant to other channels. Further report showed that the activation of transient receptor potential cation channel, subfamily A, member 1 (TRPA1) channel, rather than TRPV1 was involved in the reversible tight junctions opening by capsaicin (Kanda et al., 2018). In their study, TRPA1 was found to be responsible for the Ca^{2+} influx and they confirmed that actin reorganization was responsible for the reversibility. TRPA1 is another ion channel in the transient receptor potential (TRP) family, and it can be activated by several electrophilic compounds (such as mustard oil) due to their binding to TRPA1 cysteine residues. Later, they also discovered that transient receptor potential vanilloid 4 (TRPV4) channel activation induced rapid Ca^{2+} influx as well as a reversible increase in paracellular permeability in MDCK II monolayers, but this was induced by a synthetic agonist GSK instead of capsaicin (Mukaiyama et al., 2019).

A recent study investigated the influence of capsaicin on the integrity of microvascular endothelial cell monolayers with murine endothelial capillary brain cells (line cEND). In this, it was also observed the redistribution of the actin skeleton. In addition, the location of Claudin-5 as well as ZO-1 was changed (Kaiser et al., 2019).

In general, the mechanism for capsaicin-induced reversible tight junctions opening is partially understood and varies in different epithelial cells.

2.3 Pickering Emulsions

Pickering emulsion (PE) is a kind of emulsion stabilised only by solid particles adsorbed at the interface between two immiscible liquids. It is now well established that these solid particles form a steric barrier at the interface, resulting in high stability against coalescence for months or even years (Monégier du Sorbier et al., 2015). Once attached to the interface, the energy needed to remove the particles may be considerably large. Depending on the size and contact angle of the particles, this energy can reach thousands of kT. Therefore, the particle absorption is considered to be irreversible in many situations (Hunter et al., 2008; Linke and Drusch, 2018). This high desorption energy is also the reason for the higher stability of PE compared to surfactant-stabilised emulsions (Zembyla et al., 2020). However, it is possible to detach these particles using external magnetic or electrically fields when magnetic or electrically polarisable particles are used as stabilizing agents in the PE (Ettelaie and Lishchuk, 2015).

Many different types of solid particles can serve as stabilizing agents such as Hydroxyapatite, silica, clay, chitosan, magnetic nanoparticles, cyclodextrin, nanotube (Yang et al., 2017). Some food-grade nanoparticles, for example, starch, soy protein, whey protein, have also been commonly used. PE, either o/w, w/o or multiple, is singled out from classical ones, by the absence of surfactants (Albert et al., 2019). Due to this, PE exhibits not only superior stability, but also low toxicity and less pollution to the environment.

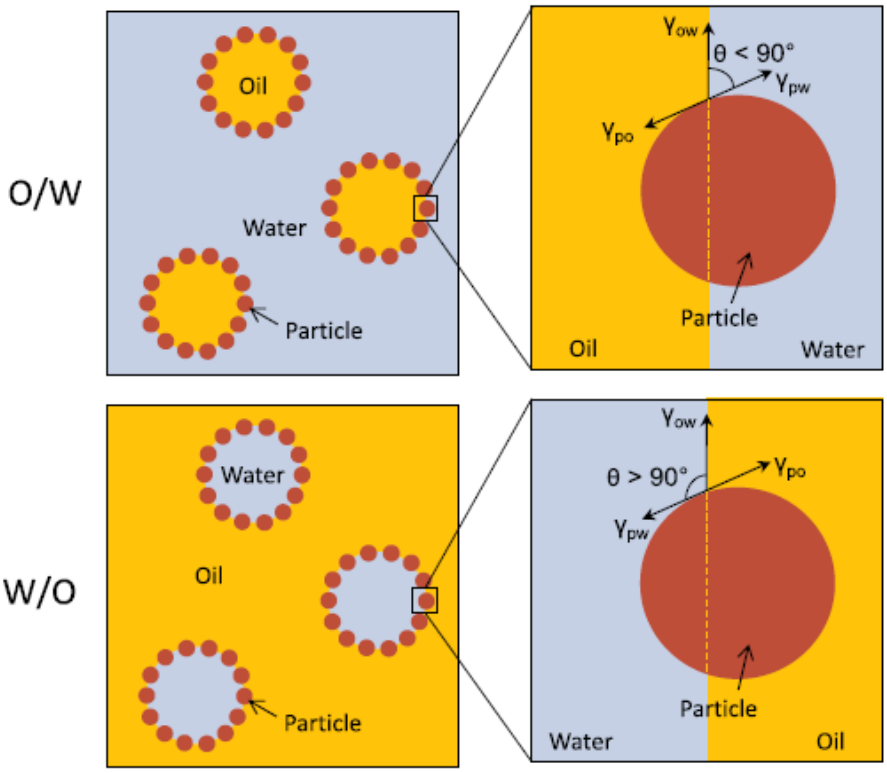

Figure 2.5 Mechanism of two types of Pickering emulsions (Albert et al., 2019).

The type of the PE formed is determined by the wettability of solid particles at the interface. The better wetting liquid becomes the continuous phase while the other one becomes the dispersed phase. The wettability of solid particles can be determined by measuring the three-phase contact angle, which is an angle measured in the water phase at the three-phase boundary of solid particles, continuous phase and dispersed phase. As Figure 2.5 shows, oil-in-water (o/w) emulsions will form if θ is less than 90◦ (e.g., silica, clay) while water-in-oil (w/o) emulsions form when θ is greater than 90◦ (e.g., carbon black). When θ is exactly 90°, particles are immersed equally into each phase and there is no preferential formation. Whether o/w or w/o emulsions result

depends on the particle and solution properties such as particle concentration (Hunter et al., 2008; Albert et al., 2019). The type of the Pickering emulsion could possibly be modified by adjusting the volume ratio of the dispersed and continuous phase (Ortiz et al., 2020). However, PE tends to be unstable when phase inversion happens.

Emulsification methods to manufacture PE were summarised and compared by Albert et al. (2019). High shear process such as high-speed homogenization, high-pressure homogenization and sonication are commonly used to produce PE. In addition, low shear techniques such as membrane emulsification and microfluidic emulsification has also been applied to prepare PE. Each emulsification technique has its own characteristics in terms of set-up, operation, emulsion properties and energy consumption. High shear process has the advantage of quick and easy set-up, while low shear techniques would benefit from better quality of the emulsion. Usually, particle characteristics such as size, polymorphism and shape are modified first by breakdown technology (bottom-up approach or top-down approach) to obtain better Pickering stabilization. And then nanoparticles are utilised to fabricate emulsions (Aditya et al., 2017).

Certain requirements in terms of wettability and size should therefore be met for these solid particles to serve as stabilizers. The size of solid particles should be smaller at least an order of magnitude than the dispersed phase in emulsion (droplets). Besides, the stability of Pickering emulsion would be affected by many parameters such as the solid particle concentration, surface charge and wettability (Chen et al., 2020).

2.4 Solvent displacement and the ouzo effect

Solvent displacement, also known as nanoprecipitation, has long been known to prepare polymeric nanoparticles (Fessi et al., 1989). It is a one-step manufacturing process with advantages such as occurring instantaneously, being reproducible and economic for the formation of nanoparticles. In addition, the nanoparticles produced are monodisperse and have a high drug loading capacity. During the process, an organic solvent that is miscible in water at all ratios is used to dissolve a hydrophobic solute. As shown in Figure 2.6, the organic phase (organic solvent + hydrophobic solute) is then injected quickly to the aqueous phase under mild stirring conditions and nanoparticles form instantly upon solvent evaporation in a rotary evaporator. The removal

of the organic solvent from nanoparticle suspension could enhance stability against Ostwald ripening and/or reduce toxic effect for biological applications (Kumar and Prud'homme, 2009).

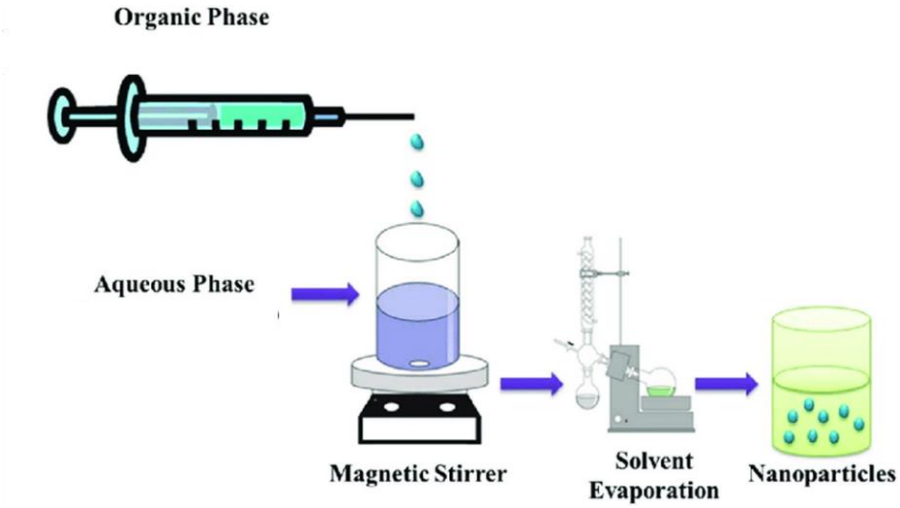

Figure 2.6 Schematic diagram of the solvent displacement method (Ye and Chi, 2018).

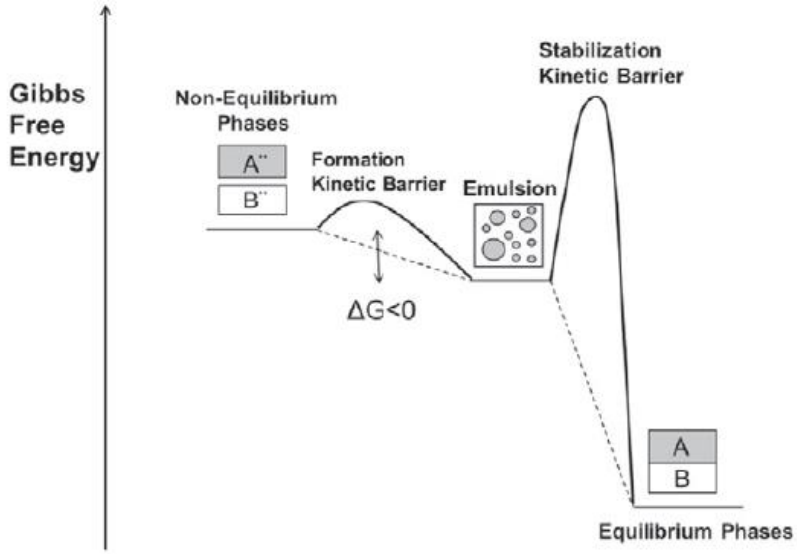

Figure 2.7 Schematic Gibbs free energy profile of spontaneous emulsification process (Solans et al., 2016).

This method requires low energy and it forms nanoparticles by spontaneous emulsification taking the advantage of internal chemical energy of the system (Anton and Vandamme, 2011). In spontaneous emulsification, as indicated in Figure 2.7, the immiscible liquids are not in equilibrium, gradients in chemical

potential between the phases may originate negative values of free energy of emulsification and emulsification is produced spontaneously.

The mechanism of nanoparticles formation was firstly explained by the well-known Marangoni effect (Fessi et al., 1989; Galindo-Rodriguez et al., 2004), which considers interfacial turbulence between two non-equilibrated phases as the driving force. Later on, the ouzo effect was discovered to describe the process of creating metastable liquid-liquid dispersions with hydrophobic solute, solvent and non-solvent, which is responsible for the turbidity appeared in some aperitifs such as Ouzo and Pastis (Vitale and Katz, 2003). This effect has been referred as the driving force of solvent displacement by recent publications (François and Katz, 2005; Beck-Broichsitter et al., 2010). Once the organic phase and aqueous phase are brought into contact, the solvent contained in the organic phase rapidly diffuses into the aqueous phase. The mixed binary solution becomes a non-solvent for the hydrophobic solute. Local supersaturation of hydrophobic solute leads to its spontaneous nucleation and growth in the form of small particles. Growth stops when the aqueous phase is no longer supersaturated with the hydrophobic solute. Polymeric nanoparticles are formed when polymers act as hydrophobic solute (François and Katz, 2005).

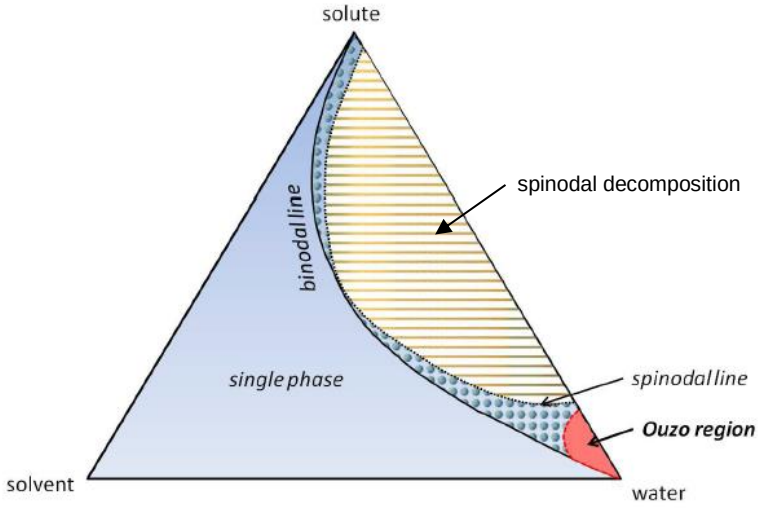

Figure 2.8 Ouzo region in the phase diagram of water, solute, solvent (Botet, 2012).

In the ternary phase diagram (Figure 2.8), the ouzo region is generally located in a very narrow area corresponding to low solute and low solvent fraction. In addition, this region is located between the spinodal and the binodal curves where a metastable dispersion can be generated. The binodal curve describes

the miscibility limit as a function of composition and it separates the conditions where are thermodynamically favourable for the system to be fully mixed (single phase region) or phase separated (two-phase region). While the spinodal curve shows the limit of thermodynamic stability with respect to small fluctuations in composition and density. Within the curve, small fluctuations would lead to phase separation via spinodal decomposition (i.e. the different pure phases appear spontaneously). Outside the curve but within the two-phase region is the metastable area, where phase separation goes by nucleation and growth (Botet, 2012; Vitale and Katz, 2003). If there are large kinetic barriers to the phase separation, it is possible for a system to exist for a long time in the metastable state, even though the Gibbs free energy is not minimized.

To determine which factor is more relevant to the solvent displacement method, a study was carried out to evaluate the effect of several parameters like: solvent type, mixing speed of polymer solution with non-solvent phase, polymer molecular weight, concentration and viscosity of polymer solutions, and interfacial tension of the non-solvent phase) on the production of nanoparticles. It was found that factors to do with the ouzo effect such as diffusion coefficient and supersaturation are more influential than interfacial tension, though they all affect the size and polydispersity during the formation and storage of particles (Beck-Broichsitter et al., 2010; Lepeltier et al., 2014).

According to previous studies (Aschenbrenner et al., 2013; François and Katz, 2005; Vitale and Katz, 2003; Lepeltier et al., 2014), two features are relevant to the ouzo effect: (1) The ouzo effect produces particles with narrow size distribution. The size of particles is determined by the concentration of solute in the organic phase, or more accurately, the ratio of excess solute to solvent. In the ouzo region, smaller particles are formed when solute concentration is lower and larger particles are formed when solute concentration is higher. This is due to the occurrence of nuclei aggregation at higher solute concentrations. More nuclei are present at higher supersaturations, resulting in larger particles. When working at lower supersaturation, nuclei are dispersed in a very diluted state so that nucleation and growth is the dominant mechanism. (2) The particles produced in the ouzo region are relatively stable without the presence of surfactant. Several factors might be involved in the stability of nanoparticles. The size of the particles is generally in the submicrometer range. Those particles are small enough so that creaming/precipitating is slow, especially when the density of the solute is close to that of water. In addition, Ostwald ripening can be greatly retarded when the solute is very

insoluble in water, the size is homogeneous and the organic solvent is removed from the aqueous phase. Besides, the further aggregation may be limited if nanoparticles display hydrophilic moieties or non- zero zeta potential (Lepeltier et al., 2014).

All in all, the ouzo effect can be taken advantage to synthesize small and stable nanoparticles with a very narrow size-dispersity. The advantages of producing nanoparticles within the ouzo region are the low energy required for their production and the absence of stabilising agent.

2.5 Cellular tight junctions

Tight junctions can be found both in the epithelium and endothelium of many tissues. In multicellular organisms, the epithelium and endothelium form physical barriers between the environment and the body. The integrity of these barriers is maintained by intercellular junctions including tight junctions, adherence junctions and desmosomes, while gap junctions are responsible for intercellular communication (Figure 2.9). Moreover, the functional barriers also regulate the transportation of essential substances across the cell layers. Figure 2.10 shows the paracellular transport along with transcellular transport (passive diffusion, transcytosis as well as carrier-mediated uptake and diffusion) that allows the selective uptake and transport. Paracellular transport is the main route for hydrophilic drugs such as peptides and proteins, while transcellular transport is the main one for lipophilic drugs (Salama et al., 2006).

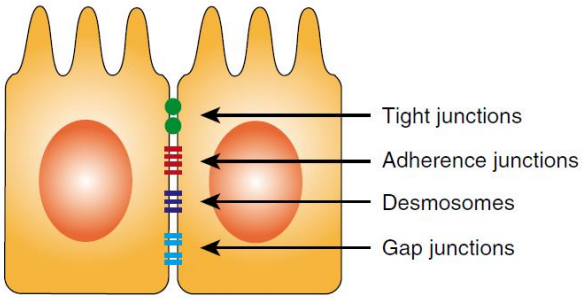

Figure 2.9 A schematic drawing of intercellular contacts between neighbouring cells forming barriers (Lea, 2015).

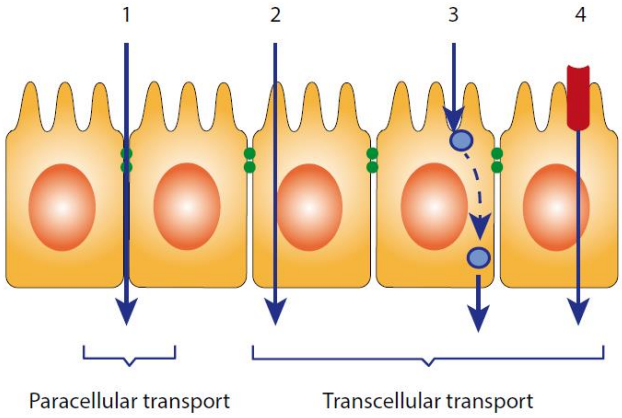

Figure 2.10 Different modes of transport through cell layers: (1) paracellular transport, (2) passive diffusion, (3) vesicle-mediated transcytosis and (4) carrier-mediated uptake and diffusion (Lea, 2015).

As the most apical part of intercellular junctions, tight junctions play an important role in sealing the paracellular space and controlling the paracellular transport of ions and molecules in a charge and size selective manner (Weber, 2012). It has been reported that solutes with molecular weights over 3.5 kDa cannot be uptake through this way, due to the dimensions of the paracellular space (Salama et al., 2006).

2.5.1 Molecular architecture of tight junctions

Tight junctions are macromolecular complexes containing more than 40 different proteins that create an interconnected network, with functions of linking adjacent cells, regulating paracellular transport as well as signalling processes such as gene expression, cell proliferation and cell polarity (Schneeberger and Lynch, 2004; Zihni et al., 2014).

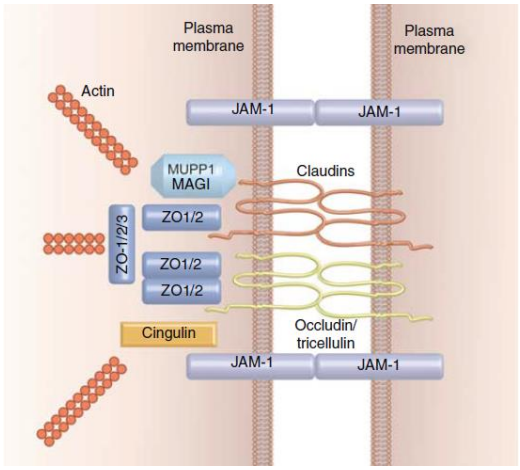

Figure 2.11 Molecular composition of tight junctions (Niessen, 2007).

Although these contain lots of proteins, the basic molecular composition of tight junctions is shown in Figure 2.11. Generally, tight junctions consist of two classes of proteins:

1) the structural transmembrane proteins which have the potential to mediate cell–to-cell adhesion;

Occludin and tricellulin, sharing similar structure, are four-span transmembrane proteins that regulate the signalling pathways of tight junctions. However, tricelluin only appears at tricellular tight junctions and it is essential for the formation of tight junction structure, while occludin is not directly involved in the barrier formation according to previous literature (Steed et al., 2009).

The claudin family (at least 24 members) also has four transmembrane domains but no sequence similar to occludin, playing a crucial role in the formation of tight junction strands, aqueous pores or channels. Different expression pattern of claudins at tight junctions are thought to be the reason for variations in the barrier property like iron or size selectivity in different epithelium and endothelium (Tsukita et al., 2001; Niessen, 2007)

The single-span protein family of junctional adhesion molecules (JAMs) is the third group of the structural transmembrane proteins. This IgG-like family may participate in cell adhesion, barrier formation or cell polarization by recruiting polarity protein complexes (Vermette et al., 2018; Niessen, 2007).

2) the scaffolding proteins which provide links between structure transmembrane proteins and actin-based cytoskeleton (Niessen, 2007).

Many different scaffolding proteins (the zonula occludens proteins, cingulin, MAGI 1–3, PAR 3/6, Pal1, PATJ, MuPP1 and others) form a cytoplasmic plaque. These proteins contain multiple interaction domains to interact directly between transmembrane proteins and actin. The zonula occludens proteins ZO-1, ZO-2, and ZO-3 are an important group of tight junctional scaffolding molecules, which can interact directly with occludin and claudins via their PDZ domains, while their C-terminus can associate with actin (Schneeberger and Lynch, 2004).

This basic structure helps to maintain the integrity of tight junctions. However, it is well known that this structure is not static and the dynamics are linked to its barrier function (Weber, 2012).

2.5.2 Enhancing drug delivery via modulation of tight junctions

While the barrier function of tight junctions contributes to the correct functioning of the organism, it is also a challenge in oral drug delivery to pass through intestinal barriers, especially for the delivery of hydrophilic drugs or macromolecules to the systemic circulation or to the central nervous system. Therefore, permeability enhancers such as surfactants (e.g. Sodium dodecyl sulfate (SDS), Tween 80), chitosan, bile acid salts, fatty acids (e.g. sodium caprate), multicarboxylic acids (e.g. ethylenediaminetetraacetic acid (EDTA)) and capsaicin are intensively studied for poorly permeable molecules (Ibrahim et al., 2020).

Ideally, a permeability enhancer should act in a non-invasive way when the drug is at the absorption site. However, most of the enhancers are targeted to increase permeability through the transcellular route, leading to mucosal damage or plasma membrane disruption (Aungst, 2012). It is important that the increase in permeability is transient and safe. Compared to the disruption of cell membrane structure, it seems that reversible opening of TJs through paracellular pathway would be safer.

Recently, some peptides derived from zonula occludens toxin, or Clostridium perfringens enterotoxin (Deli, 2009; Bocsik et al., 2016), chitosan (Yeh et al., 2011), capsaicin (Shiobara et al., 2013; Kaiser et al., 2019) have been confirmed for their ability of mediating reversible opening of tight junctions. These kind of modulators can enhance drug delivery across epithelial barriers and the blood–brain barrier. They can also provide a potential way to enable the oral administration of proteins and peptides.

2.5.3 Methods to investigate integrity of cellular tight junctions

Since tight junctions regulate the paracellular transport, it is necessary to assess the cell permeability and drug absorption under different stimulus. Therefore, different types of techniques have been developed to evaluate the integrity of tight junctions.

Transepithelial/transendothelial electrical resistance (TEER) measurements are frequently used to quantify the integrity of cellular barriers. TEER primarily reflects the permeability of paracellular pathway to ions like Na^+, Cl^-, K^+ and $HCO3^-$. This measurement can be conducted on cells growing on filters with a voltohmmeter and a pair of chopstick-style electrodes. But it has some drawbacks, for example, TEER values measured with this device depends on the position of the electrodes, and it may cause disturbance to cells when

inserting them into the wells. Also an overestimation of TEER could happen due to the inhomogeneity of the electric field produced by chopstick-style electrodes across the cell layers. This can be reduced by the central placement of electrodes, an increase in the medium volume and using inserts with smaller area (Jovov et al., 1991). In addition, using an EndOhm chamber to measure TEERs is more reliable as the device provides a more uniform current density compared to handheld chopstick electrodes (Sheller et al., 2017).

Compared to voltohmmeter, impedance spectroscopy is a more advanced method to assess ion permeability, which analyses signal with a frequency sweep rather than a single fixed frequency (Srinivasan et al., 2015). Therefore, it can provide not only the TEER values but also the capacitance. Besides, it is non-invasive and automated. In this, cells are grown on permeable membranes to form monolayers and then transferred to a multi-well device to perform electrical measurements by placing an electrode on each side of the membrane and applying an AC voltage with a range of frequencies. Figure 2.12A shows how the TEER, capacitance of the monolayer (C_{Cl}), ohmic resistance of cell medium (R_{medium}) and capacitance of the electrodes (C_{El}) contribute to the total impedance of the system. Based on the equivalent circuit (Figure 2.12B), the computer software can calculate and process the TEER and capacitance as readout parameters.

There is an obvious correlation between permeability and TEER: tight cell monolayers correlate with high values of TEER while high permeability monolayers show low TEER values. As for the capacitance (C_{Cl}), it gives additional information about the morphological changes and cell detachment. Besides, cell viability can be estimated from the change in capacitance (Benson et al., 2013; Lee et al., 2012).

However, the methods mentioned above do not discriminate between the paracellular and transcellular pathway. This is very important when ion fluxes via ion channels are involved in the process. Researchers have developed a two-path impedance spectroscopy to differentiate between these two pathways by reversible modulation of the paracellular pathway combined with flux measurements of fluorescein as a paracellular marker (Krug et al., 2009).

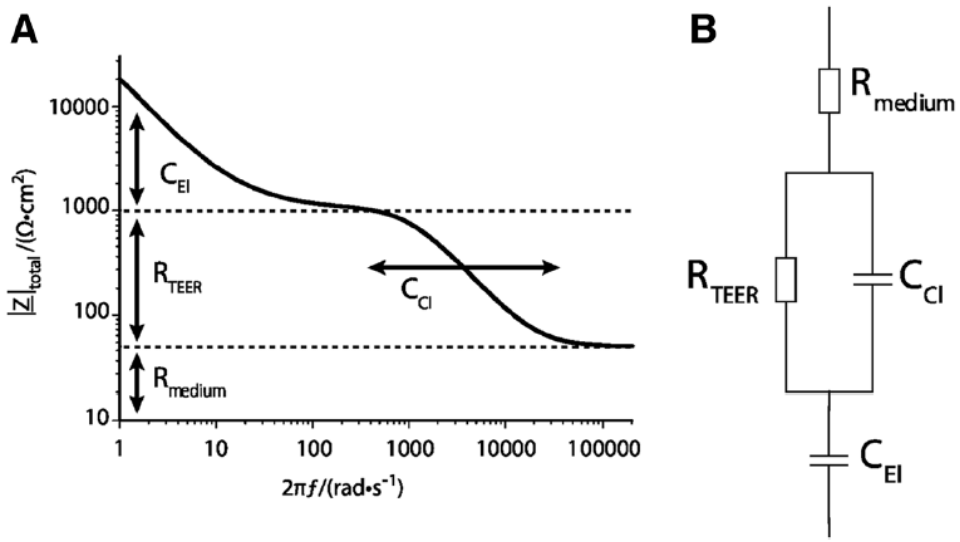

Figure 2.12 Typical impedance spectrum of a cell monolayer at different frequencies (A) and the equivalent electrical circuit diagram (B). Z, the total impedance; C_{El}, capacitance of the electrodes; C_{Cl}, capacitance of the cell monolayer; R_{medium}, ohmic resistance of the medium; R_{TEER}, ohmic resistance of the cell monolayer (Benson et al., 2013).

Another method to investigate epithelial/endothelial barrier integrity is to determine the permeability of certain hydrophilic substrates of varying molecular weights, such as sucrose or dextran. Radioactive or fluorescently-labelled substrates are preferred for easy analytical detection (Benson et al., 2013). Permeability coefficient can be calculated to quantify the barrier function. The permeability can be tested in two directions, from the apical side to the basolateral side or vice versa. Transcellular pathways must be excluded by specific inhibitors. Due to the non-invasive nature of TEER measurements and their outstanding temporal resolution, the impedance spectroscopy is often favoured over permeability assays to ensure barrier integrity.

In addition, there are many advanced imaging techniques investigating the opening phenomenon itself. Electron microscopy and freeze fracture electron microscopy are useful techniques for ultrastructural characterisation of the tight junctions. When combined with immunolabeling, they can also be used for protein localization (Johnson, 2005). High-resolution fluorescence microscopy such as laser scanning confocal microscopy, has also been attractive for the visualization of immuno stained tight junctions (Markov et al., 2012).

2.6 Aim of the project

Capsaicin is a multi-functional active compound with many biological exhibited applications, especially its potential application as a paracellular permeability enhancer. However, the application of capsaicin has some drawbacks regarding its low water solubility, cytotoxicity at high doses and pungency. Thus, many delivery systems have been developed to encapsulate capsaicin in order to improve its oral bioavailability while at the same time attenuating their irritating and sensitizing capacity.

Pickering emulsification, in which solid particles adsorb at in the interface to stabilise emulsions, is a well-known technology conferring high resistance to coalescence due to steric barriers formed by the solid particles. With the use of edible, biodegradable and biocompatible solid particles, Pickering emulsions have great potential to be used as therapeutic vehicles for drug delivery. Usually solid particles using as Pickering emulsifiers have to be modified first to decrease their large particle size and their irregular morphology to increase its efficiency to stabilise the emulsion. Pickering emulsions generally require high shear processes for their formation. The use of capsaicin nanoparticles to stabilise emulsions has not been reported yet.

Solvent displacement is generally a simple, fast and spontaneous process to produce nanoparticles. Under appropriate conditions, highly monodispersed, small and stable nanoparticles can be synthesized. The ouzo region identified within the ternary phase diagram satisfy such conditions. Normally, three compounds are involved in this process, the hydrophobic solute, solvent and non-solvent. The addition to the system of another hydrophobic solute such as oil renders a more complex system.

Given the above background, the aim of this project is to evaluate the suitability of capsaicin nanoparticles to stabilise the o/w Pickering emulsion. It was hypothesized that when capsaicin and oil are both introduced into the system, given the insolubility of capsaicin in oil, the formed capsaicin nanoparticles during the process could potentially act as emulsifier by adsorbing at the oil and water interface. This would provide a novel way to produce Pickering emulsions avoiding the use of high shear energy. The project also aimed to examine whether the obtained capsaicin-stabilised NE influence the tight junctions of MDCK II cell monolayers.

To achieve the above aim, the work is divided in the following parts:

1) A study of the solubility, phase equilibrium and recrystallization of capsaicin in binary solvent mixtures of ethanol and water;

2) Development of capsaicin nanoemulsions by Pickering stabilisation harnessing the nanoprecipitation and the ouzo effect;
3) Preliminary assessment of the effect of capsaicin nanoemulsions on the permeability of epithelial monolayers of MDCK II cells.

Chapter 3
Materials and Methods

3.1 Materials

Capsaicin was purchased from two different suppliers Hello Bio (Bristol, UK) & Sigma-Aldrich (from Capsicum sp. 95%, Steinheim, Germany). FTIR and HPLC analysis showed both compounds are identical. Capsaicin from Sigma-Aldrich was used for all studies except turbidity study and characterisation of capsaicin nanoparticles, in which capsaicin from Hello Bio was used. Pharmaceutical grade Miglyol®812, a mixture of medium-chain triglycerides, was from Sigma-Aldrich (St Quentin-Fallavier, France). Ethanol absolute was from VWR Chemicals (Lutterworth, UK). Milli-Q water, used throughout, was from a Milli-Q Gradient water purification system (Millipore, Watford, UK).

3.2 Methods

3.2.1 FTIR and HPLC analysis of capsaicins from two suppliers.

Capsaicins from two suppliers were evaluated by Fourier transform infrared spectroscopy (FTIR) and high-performance liquid chromatography (HPLC). The FTIR measurements were performed between 650 and 4000 cm^{-1} at 1 cm^{-1} spectral resolution using a 4500 series portable FTIR Spectrometer (A2 Technologies, Danbury, USA). The data collection and analysis were conducted using the Microlab PC software. 400 µg/mL of capsaicin-ethanol solution was prepared with each capsaicin for HPLC analysis as described in section 3.28.

3.2.2 Solubility study of capsaicin in solvent mixtures.

The equilibrium for capsaicin dissolved in binary solvent mixtures of ethanol and water were studied at 25°C under atmospheric pressure. The temperature was controlled using a water bath (Grant Instruments Ltd, Cambridge, UK) and high performance liquid phase chromatography (HPLC, Shimadzu) was employed for capsaicin detection in solution.

An excess of capsaicin (an amount above the maximum solubility of capsaicin) was added to a glass vessel with a cap containing pure Milli-Q water at first.

This was kept under magnetic stirring (LTE Scientific Ltd, Oldham, UK) set at speed level 2 according to the dial selector switch during 3 h to ensure equilibrium was reached. Then the saturated solution was allowed to stand for about 1 h to enable any solids that were finely dispersed in the solution to settle down. An aliquot of 400 µL from the supernatant was taken out while being weighed on a 0.1 mg precision balance. Mass of the sample was recorded. The aliquot was then filtered through 0.2 µm PTFE syringe filters (fisherbrand^{TM}, Fisher Scientific UK Ltd, Loughborough, UK). The sample was diluted with ethanol to keep all components in solution.

To adjust the mass fraction of ethanol (0.1) in the solvent mixture, the required mass of ethanol to add can be calculated as follows:

Mass of ethanol to add = mass of the solvent mixture after sampling(3054.4) × mass fraction of water (1) / mass fraction of water (0.9) – mass of the solvent mixture after sampling(3054.4)

Ethanol was then added while being weighed in order to record the actual mass of ethanol added. The actual mass fraction of ethanol cam then be calculated as follows:

Mass fraction of ethanol = (Mass of the solvent mixture after sampling (3054.4) × mass fraction of ethanol (0) + mass of ethanol added (323.3)) / mass of the solvent mixture (3377.7)

The system was stirred for another 3 h. Sampling taking a 400 µL was then performed as protocol described above. Experimental data were recorded in Table 3.1. After finishing all the tests, the samples were injected into an HPLC system to determine the concentration of capsaicin in solution.

Table 3.1 Data of binary solvent mixtures of ethanol and water.

Mass fraction of ethanol	Mass of ethanol added (mg)	Mass of the solvent mixture (mg)	Mass of the sample (mg)	Mass of the solvent mixture after sampling (mg)
0	-	3453.0	398.6	3054.4
0.096	323.3	3377.7	389.9	2987.8
0.200	389.1	3376.9	383.2	2993.7

3.2.3 Capsaicin nanoparticles preparation

Capsaicin was firstly dissolved in ethanol at three different stock concentrations (1.25 mg/mL, 2.3 mg/mL and 10 mg/mL). A certain volume of capsaicin ethanol solution was added into an Eppendorf tube containing water and then mixed by pipetting up and down for 10 times at room temperature. The total volume was 200 μL for turbidity measurements and 300 μL for size characterisation.

3.2.4 Turbidity measurements

Samples were transferred to a flat base transparent 96-well plate (SARSTEDT AG & Co, Nümbrecht, Germany) with 200 μL per well for all the measurements. Turbidity was measured at 25°C through the detection of absorbance of light scattered at 600 nm (OD_{600}) using a microplate reader (Tecan Group Ltd., Männedorf, Switzerland).

3.2.5 Nanoemulsions preparation

Table 3.2 Formulations of capsaicin-loaded NEs.

No.	Capsaicin concentration (mg/mL)	Capsaicin solution (μL)	Water (μL)	Miglyol®812 (μL)
1	1.25	896	9063	41
2	1.25	1295	8664	41
3	1.25	1660	8299	41
4	2.3	896	9063	41
5	2.3	1295	8664	41

Capsaicin was dissolved in ethanol at a concentration of 2.3 mg/mL. Briefly, a specific volume of Miglyol®812 was mixed with a specific volume of capsaicin-ethanol solution first to form the organic phase (see Table 3.2). This was immediately poured into a large amount of water according to Table 3.2 in a beaker under magnetic stirring (US 152, Stuart Equipment, Stone, UK) at speed level 4 at room temperature. The magnetic stirring is conducted for 10

min with a parafilm covering the beaker to prevent ethanol evaporation. Then the emulsion (milky dispersion) was concentrated in a rotary evaporator (Heidolph Instruments, Schwabach, Germany) at 35°C until reaching a desired volume of nanoemulsions to yield a final capsaicin concentration of ~ 2.5 mM.

3.2.6 Particle size distribution and Zeta potential analysis

The particle size distributions, the mean particle diameter and the polydispersity index (PDI) of all nano-formulations were measured by dynamic light scattering (DLS) using a Malvern Zetasizer Ultra (Malvern Instruments Ltd., Worcestershire, UK) at 25°C. Measurements were carried out using disposable cuvettes and at 173° angle. Samples were diluted with Milli-Q water prior to being tested.

Zeta potentials were measured at 25°C using a disposable folded capillary electrophoretic cuvette (DTS1070, from Malvern Instruments Ltd., Worcestershire, UK) by mixed laser Doppler velocimetry and phase analysis light scattering (M3–PALS).

A refractive index of 1.51 was used for capsaicin and 1.44 for Miglyol®812. All measurements were performed in triplicate.

3.2.7 Transmission electron microscopy (TEM)

The morphology and size of the NE was analysed by TEM at the Astbury Centre for Structural and Molecular Biology of the university of Leeds. TEM was performed using a JEM-1400 Transmission Electron Microscope (JEOL USA, Inc., Peabody, USA), running with a tungsten filament at 120 kV. The images were captured on a Gatan 1 K CCD camera.

In order to increase the electron contrast, the samples were prepared via negative staining. Briefly, 5 µL of the NE was pipetted onto a 3 mm diameter, carbon coated, copper TEM grid. This was left for 1 minute to allow the particles to adhere to the carbon film. A piece of Whatman no.1 filter paper was used to wick away the excess of liquid from the sample and a 5 µL drop of 1% uranyl acetate stain was deposited onto the sample and excess of liquid again wicked off after 10 s.

3.2.8 High-performance liquid chromatography (HPLC) with UV and fluorescence detection

HPLC measurements were carried out using a Shimadzu Prominence HPLC System (Shimadzu, Columbia, USA) comprising a model DGU-20AS degasser, a LC-20 AD pump system, a SIL-20 AC auto-sampler, a CTO-20AC column oven, a photodiode array detector system (SPD-20A) and a RF-20Axs fluorescence detector.

Capsaicin was separated on a Kinetex C18 reversed phase column (5 µm, 100 Å, 150×4.6 mm, 00F-4601-E0; Phenomenex, Torrance, USA). Temperature in the oven was set to 30°C and the flow rate was set to 1.0 mL/min. A mixture of water and 20% (v/v) acetonitrile was used in isocratic mode as the mobile phase. The mobile phase gradient was set as displayed in Table 3.3. The injection volume was 20 µL. The detection wavelength was set at ch1: 282 nm, wavelength ch2: 360 nm for UV detection and excitation wavelength of 280 nm and emission wavelength of 320 nm were set respectively for fluorescence detection. The retention time of capsaicin was at around 5.9 min. The software used to operate the system was LabSolutions. The calibration curve prepared using standard solutions of capsaicin was linear ($R^2 = 0.999$) in the concentration range of 30 - 600 µg/mL.

Table 3.3 Mobile phase gradient for HPLC capsaicin method.

Time (mins)	% Water	% Acetonitrile
0	55	45
8	50	50
15	45	55
40	10	90
45	55	45
55	55	45

3.2.9 Determination of association efficiency

The nanoemulsions were partitioned using Viva Spin tubes (Vivaspin turbo 15 PES 30KD, Sartorius) by centrifugation (Rotina 380, Hettich GmbH & Co. KG, Tuttlingen, Germany) at 3000 g-force for 1 h at 20 °C. The liquid passing

through the membrane of vivaspin was collected and then filtered through a 0.2 µm PTFE syringe filter (fisherbrand™, Fisher Scientific UK Ltd, Loughborough, UK). HPLC system was used to accurately quantify the amount of free capsaicin in solution. The association efficiency (AE) of capsaicin was calculated as follows:

AE (%) = (Total capsaicin amount − Free capsaicin amount) × 100 / Total capsaicin amount

3.2.10 Emulsion stability tests

The stability of nanoemulsions under storage at room temperature was tested. Both particle size and zeta potential were tested during five days.

3.2.11 Cell culture

Madin-Darby Canine Kidney (MDCK) II cells (Batch 19G037, P-30) (ECACC, public Health England, Salisbury, UK) were cultured in 75 cm^2 flasks using DMEM (Invitrogen, Carlsbad, CA) supplemented with 5% FBS (Fetal bovine serum) and 1% PEST (penicillin-streptomycin, 10000 units penicillin, 10000 units streptomycin in 0.9% NaCl). The cultures were maintained in an incubator at 37°C with 5% CO_2 (MCO-18AIC, Sanyo Electric Co., Ltd, Osaka, Japan). Cells from passages 31-38 were used for all experiments. After reaching microscopic confluence, the cells were washed with 10 mL phosphate buffered saline (PBS) twice and trypsinized for 6 min with 8 mL 0.05% trypsin in EDTA (1X) buffer. After detachment, 10 mL of cell culture medium was added to the trypsin buffer. The cell suspension was then centrifuged at 2000 rpm for 5 min (Universal 320 R, Hettich GmbH, Tuttlingen, Germany). The medium was removed and the cell pellet was resuspended in cell culture medium. A 45 µL aliquot of cell suspension was diluted with 5 µL trypan blue and the number of cells was counted with an improved Neubauer chamber. The cells were then sub-cultured.

3.2.12 Electrical impedance measurements

Transepithelial electrical resistance (TEER) and capacitance (C_{CL}) of cell monolayers were measured using an automated CellZscope® instrument (nanoAnalytics, Münster, Germany). Cells were grown on translucent transwell permeable supports (12 mm, 1 cm^2 growth area, 0.4 µm pore size; Corning Inc., New York, USA). The supports were pre-wet with about 0.1 mL of cell culture medium for at least 2 min. 1.5 mL of cell culture medium was

transferred to the basolateral chamber. A 500 µL aliquot of MDCK II cells in suspension was then seeded onto the membrane of the supports (~10^5 cells per well). The plate was incubated with the supports at 37 °C and 5% CO_2 in a humid atmosphere for 6 h (if seeding was carried out during the morning) or 16 h overnight (if the seeding was carried out at the end of the day). After this, the apical medium was removed and replaced with 0.7 mL of cell culture medium in order to remove non-adherent cells and reduce the risk of multilayer formation. Each well in the instrument was then filled with 1.5 mL of cell culture medium. The supports were finally transferred into the instrument to monitor the growth of cells and the formation of the monolayer.

Before the cells reached confluency, the medium of the supports was replaced in the apical compartment as well as in the wells with pure DMEM. Once constant resistance was reached of at least 100 Ω/cm^2 , the experiment was started by replacing 350 µL of the medium in the apical chamber with the sample dissolved in pure medium at double the desired concentration. Control samples consisting of pure DMEM were used as a mean of reference. The resistance and capacitance were measured continuously for 24 h.

3.2.13 Data analysis

Data statistical analysis was carried out using Microsoft Excel v16.0.13628.20318 (64 bit) and Origin 2020. SpectraGryph v1.2 was used for the analysis of FTIR. All experiments were conducted at least in triplicate except the solubility tests and the impedance measurements.

Chapter 4
Results and Discussion

4.1 FTIR and HPLC analysis of capsaicins from two suppliers

FTIR and HPLC studies were performed to compare the analytical characteristics of the capsaicins obtained from two different suppliers. FTIR spectra of capsaicins are shown in Figure 4.1. The FTIR spectrum of capsaicin from Sigma showed the appearance of peak at ~3310 cm^{-1} characteristic of secondary amine ν(N-H) and ν(O-H), ~3000 and ~2840 cm^{-1} assigned to aliphatic ν(C-H), ~2850 cm^{-1} assigned to ν(C-H) in methyl ester and 1627 cm^{-1} for ν(C=O), ~1630 to ν(C=O) of amide I and ~1525 cm^{-1} for δ(N-H) and ν_s(N-C=O) of amide II, and 1238 cm^{-1} for ν(C-N), 1260 cm^{-1} assigned to ν(C-O) in aromatic-OH, ~990 cm^{-1} assigned to δ_{oop}(C=C). The region of 1000 to 500 cm^{-1} shows "fingerprint" bands characteristic of asymmetric tri-substituted aromatic ring. Overall, very similar FTIR spectra were determined for the two capsaicin samples indicating a consistent with structure on both. The spectra of capsaicin are also consistent with those presented in the literature (El-Kaaby et al., 2016; Giri et al., 2016; Tran and Hadinoto, 2017).

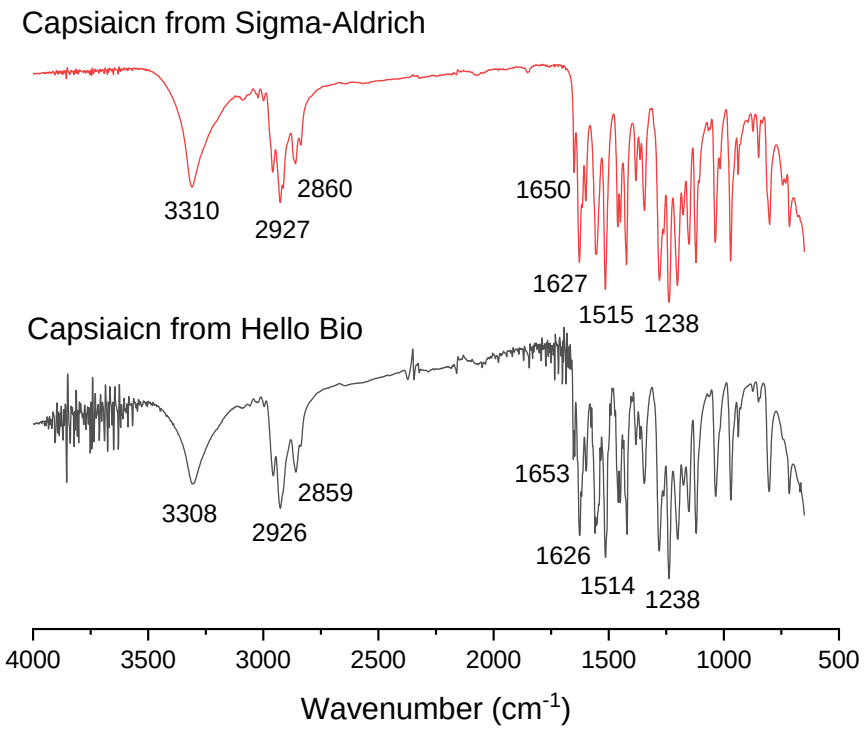

Figure 4.1 FTIR spectra of the capsaicins from two suppliers: Sigma-Aldrich (red line) and Hello Bio (black line).

As for HPLC analysis, the peaks of interest corresponding to capsaicin were identified in the chromatograms (Figure 4.2) obtained for two capsaicins. An extra peak was observed in the Chromatogram (Figure 4.2b) of capsaicin from Hello Bio, this corresponds to dihydrocapsaicin, indicating a lower degree of purity of the compound produced by this supplier. The retention time for capsaicin and dihydrocapsaicin was 5.83 and 7.42 min, respectively. According to the chemical structure shown in section 2.2.1, capsaicin and dihydrocapsaicin are only different in one unsaturation in the aliphatic chain, therefore, the FTIR spectra did not show any significant difference.

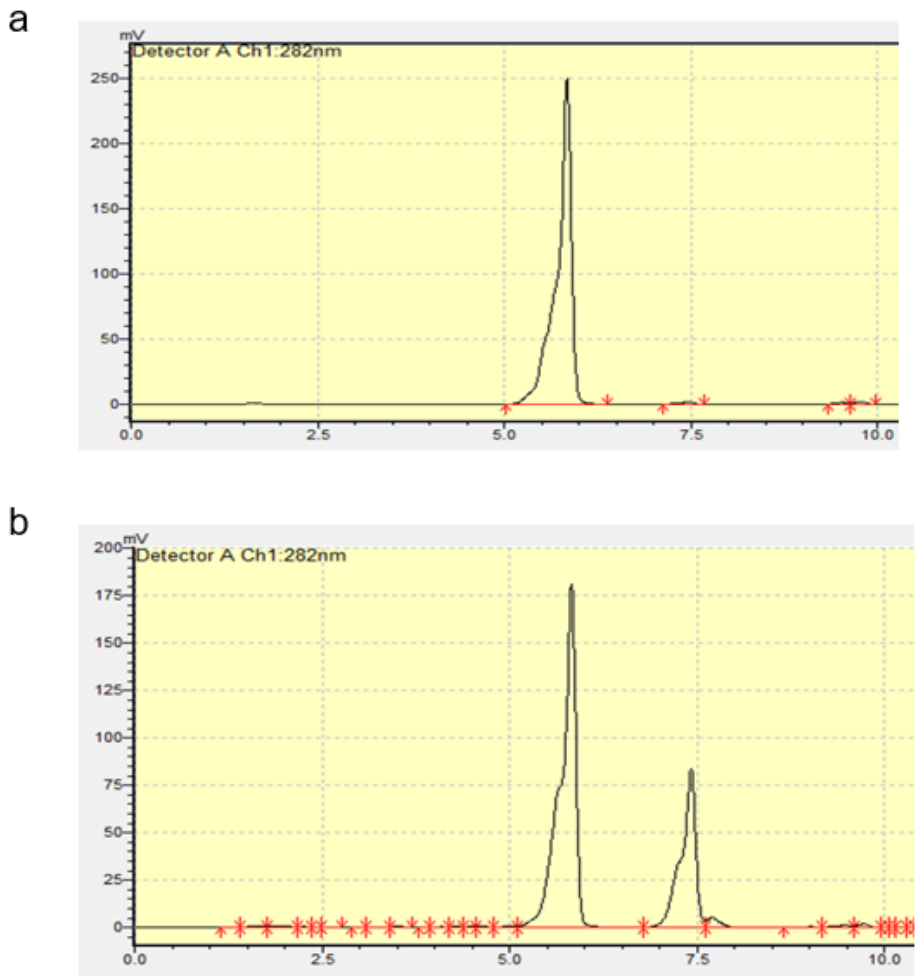

Figure 4.2 Chromatograms of the capsaicin-ethanol solution at 400 µg/mL, (a) capsaicin from Sigma-Aldrich; (b) capsaicin from Hello Bio.

4.2 Solubility study of capsaicin in solvent mixtures

According to the product information from Cayman Chemical, the solubility of capsaicin is at least 30 mg/mL in ethanol (Cayman Chemical, 2020). But it has been reported to have a lower solubility of 28.93 mg/L in water at 25°C (Gv et al., 2018). However the solubility of capsaicin in a mixture of solvents (ethanol of water) has not been previously reported to our knowledge. In this work the solubility of capsaicin in a mixed solvent system of ethanol and water was evaluated. Table 4.1 displays the measured values of solubility of capsaicin at 25°C in binary solvent mixtures at different mass fractions of ethanol. As expected, the solubility of capsaicin increases along with the increase of ethanol composition in the solvent mixture.

Table 4.1 Experimental solubility of capsaicin at 25°C in binary mixture of solvents (ethanol+ water) at different mass fraction ratios.

Ethanol mass fraction	Water mass fraction	Solubility of capsaicin (mg/L)
0.000	1.000	17.89
0.096	0.904	137.40
0.200	0.800	580.78

As it can be seen from Table 4.1, the maximum solubility of capsaicin in water in a supersaturated conditions was determined as 17.9 mg/L that is lower than that reported. The solubility information is very important for the development of the recrystallization process of capsaicin and to tailor the crystal formation in terms of size and PDI. A previous study reported the experimental data on solubility of capsaicin in different pure solvents such as n-hexane, cyclohexane and carbon disulfide (Yan et al., 2012). Other research works have also compared the solubility of capsaicin in solutions of varying percentages of ethanol via UV/Vis detection (Costanzo et al., 2014). However, this is the first time where data on the solubility of capsaicin in binary solvent mixtures by HPLC is reported. The purpose of this study was to tailor the synthesis of highly monodispersed capsaicin nanoparticles through its recrystallization. A stirring period of 3 h to perform the solubility tests was deemed enough to reach equilibrium conditions within the system in terms of the final application purposes in this study. Longer times of contact

and wider range of temperatures would be required for a thorough theoretical study (Tsavas et al., 2002).

Interestingly, when there is around 30% (m/m) of ethanol in the mixture, the appearance of two liquid phases can be observed under constant stirring. As it is shown in Figure 4.3a, an excess of capsaicin leads to the dispersion of droplets (circled in yellow) floating on the surface of the supersaturated solution rather than to the dispersion of solid particles. Once the system is left to cool down and the stirring is stopped, the system then becomes cloudy and develops a milky appearance within several minutes (Figures 4.3b and c). It finally becomes phase separated, leading to the formation of needle-like capsaicin crystals. This last process occurs within a period of several hours (Figure 4.3d).

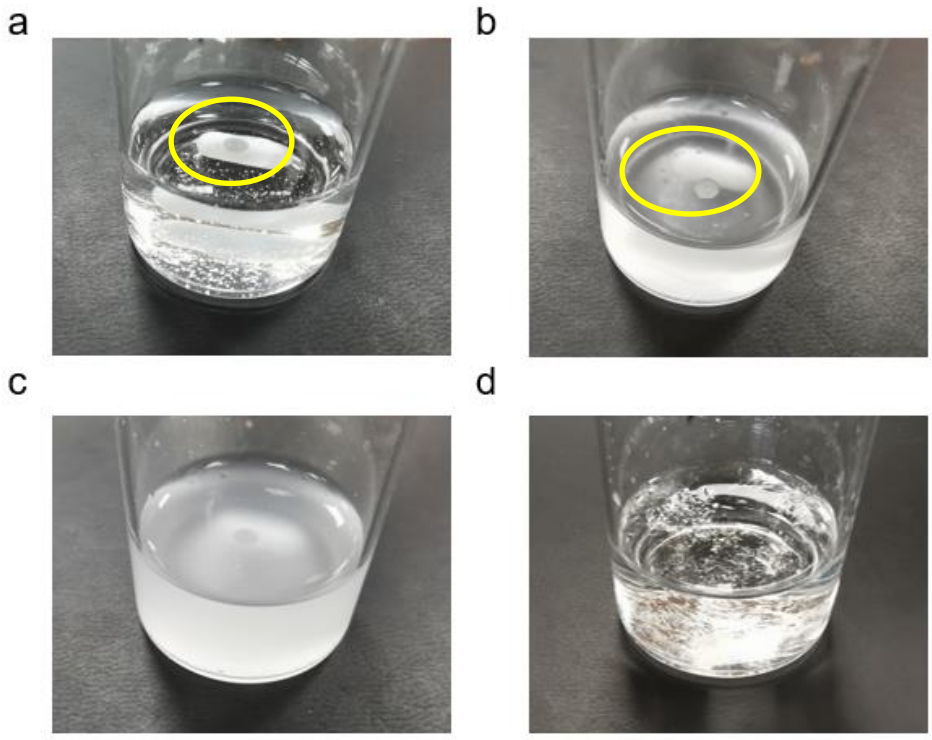

Figure 4.3 Phase transition of the system with around 30% ethanol in the solvent mixture. (a) the appearance of two liquid phases under constant stirring; (b and c) the milky white appearance of the system when self-cooling and the stirring is stopped; (d) the formation of needle-like capsaicin crystals after several hours.

The appearance of capsaicin-rich, oily droplets on the liquid surface, though no oil was added in this case, could probably be explained by the oiling out

behaviour of capsaicin. Oiling out, also termed out as liquid-liquid phase separation, has been reported for many proteins, polymers and small organic molecules especially APIs during crystallization (Meng et al., 2020; Zhang et al., 2021). Normally, crystallization from solution follows crystals nucleation and growth, while in some cases, an intermediate liquid-like state occurs prior to crystal nucleation and the crystal nuclei start to form in those droplets (Sun et al., 2018). It usually happens during the cooling crystallization using a mixture of solvents when the supersaturation degree is too high (Takasuga and Ooshima, 2014). Oiling out is normally undesirable since it causes problems in crystal purity, morphology and size distribution; however, recent researches have shown this phenomenon can be controlled to produce spherical crystals (Bonnett et al., 2003). In our case, the system existed as two liquid phases with one phase dispersed in the form of droplets under constant stirring. Some small crystal nuclei could have been formed in these droplets at the beginning since they look turbid, but longer time is required for crystal growth.

As for the system transition, the underlying mechanism could be that the system falls into metastable state due to the change in temperature, leading to the nucleation of capsaicin in the continuous phase. The appearance of turbidity (milky like colour) may be as result of light scattering effect by those small nucleus. However, those crystals will continue to grow and aggregate forming more stable needle-like crystals and the solution becomes transparent again. With the cap on the glass vessel, it can be assumed that ethanol was not evaporating here. This process resembles the ouzo effect but exhibits low stability that develops with time.

4.3 Phase equilibrium study of capsaicin nanoparticles formation

Making use of what appeared to be the formation of capsaicin crystals (capsaicin nuclei) as described earlier in section 4.1 resembling the ouzo effect, the recrystallisation process was studied under different conditions such as different ratios of water to ethanol (WER) and varying the concentrations of capsaicin present in the system.

A ternary phase diagram of the system water-ethanol-capsaicin was built in attempt to identify the ouzo region. Since capsaicin is not soluble in water, the phase diagram can be divided into two parts according to the well-known

binodal line, which separates the one-phase region from the two-phase region. That line indicates the limit in the solubility of capsaicin in the mixture of water and ethanol, which can be converted using the solubility data.

Turbidity measurements were carried out over time to understand the phase behaviour and stability of systems at different water to ethanol ratios (WER) and then at three different capsaicin concentrations (1.25, 2.3 and 10 mg/mL). In addition, the region of interest was investigated corresponding to where nano-sized, highly monodispersed and stable capsaicin nanoparticles were formed.

Figure 4.4 shows that the absorbance (proportional to the turbidity) of the system, showed a general trend to increase considerably first and then decrease along with the decrease of WER (increase of ethanol content) at all capsaicin concentrations. This was because the level of supersaturation of capsaicin was greatly influenced by variations in WER. Those samples with smaller WER (higher ethanol concentration) exhibited the smallest absorbances (around 0.04), which could mean the existence of one phase in the system where capsaicin present in the system is fully soluble in the mixture of water and ethanol. As for higher WER (higher water concentration), the values of absorbance became smaller again because of the smaller amount of ethanol incorporated, leading to the formation of smaller amount of capsaicin crystals in the system. Thus, each concentration of capsaicin had a given WER leading to the highest turbidity and therefore the formation of dispersed nanoparticles. When looking at the same WER, higher capsaicin concentrations led to higher values of absorbance. Though the values of absorbance for systems with the smallest capsaicin concentration (1.25 mg/mL) were relatively low, capsaicin concentrations were above the solubility limit of the binary solvent mixture at higher WER, since the solubility of capsaicin in water is extremely low. The small changes in the absorbance values along with time can be explained by the unstable nature of the systems possibly associated with the evaporation of some ethanol and/or the growth or aggregation of the nanoparticles.

High turbidity in the system could either mean a larger amount of capsaicin dispersed nanoparticles or larger size of capsaicin nanoparticles since absorbance is a parameter that measures the attenuation of the transmitted light within the material. Attenuation can be caused by different physical process such as absorption by the sample, reflection loses and particles light scattering.

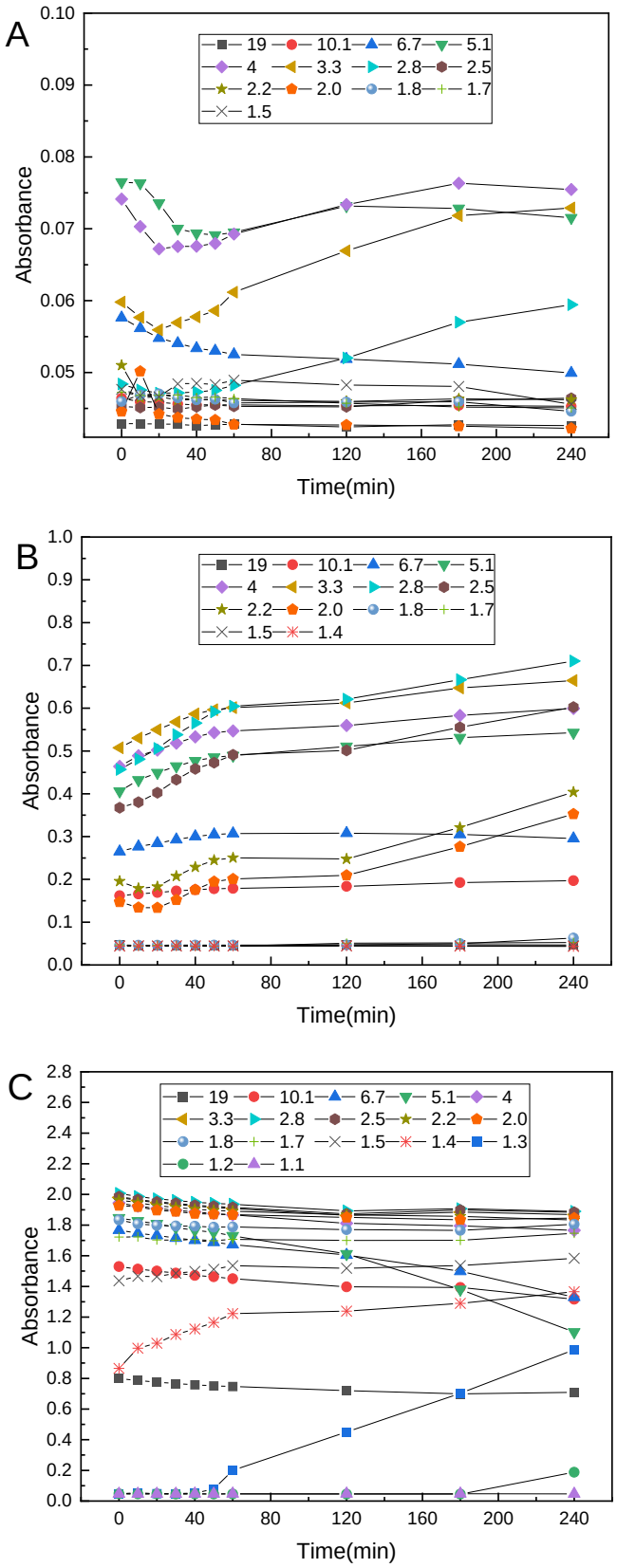

Figure 4.4 Effect of water-to-ethanol ratio (WER) on the absorbance (measured at 600 nm) of systems over time at three different capsaicin concentration (A: 1.25 mg/mL, B: 2.3 mg/mL, C: 10 mg/mL). Different symbols represent varied WER.

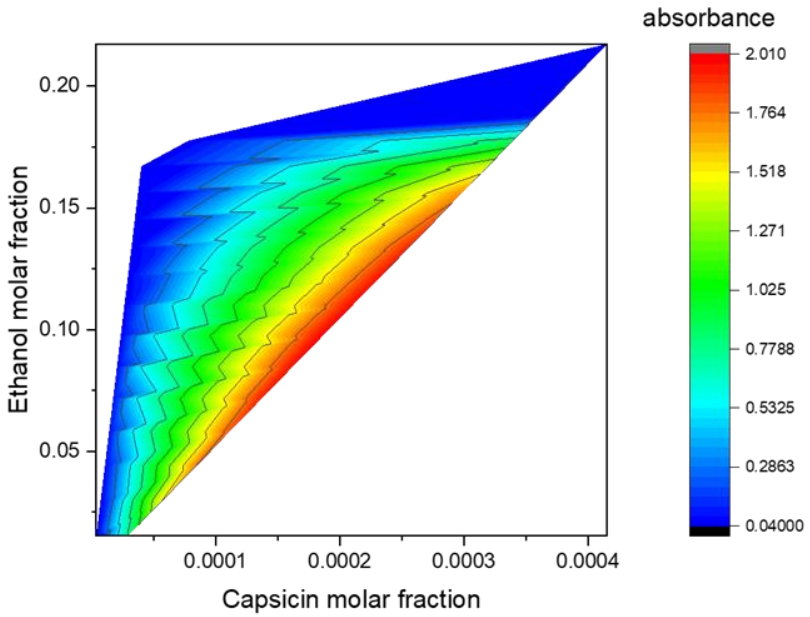

Figure 4.5 2D contour plot showing the dependence of the absorbance (measured at 600 nm) as a function of the ethanol and capsaicin molar fractions at 0 min. The region with no data was not explored.

Figure 4.5 shows a 2D contour plot for turbidity. The dark blue area and above region corresponds to the region where one-phase is predominant, this occurs at higher level of ethanol or low capsaicin content. The orange area highlights the region where nucleation is likely to occur due to supersaturation, leading to formation of large amount of capsaicin crystals and even non-soluble solid capsaicin.

Based on the analysis of above diagrams, several formulations that showed low variation of absorbance along time were selected for particle size distribution analysis via dynamic light scattering (DLS) and only 5 of them (Table 4.2) showed smaller particle size ranging from 100 to 500 nm and having low PDI values (< 0.2). These particles became larger in size when measured after 2 h at room temperature, indicating the growth of nanoparticles. The size of the capsaicin nanoparticles could be controlled to produce nanoparticles between 100 and 500 nm by changing the concentration of the initial solution since they all had a very high WER. As suggested in previous works where ouzo region has been studied, the use of higher solute concentrations leads to larger size particles. In this case, more nuclei are produced by a higher level of supersaturation and these nuclei aggregate instead of growing by diffusion, resulting in larger particles at higher supersaturations (Aschenbrenner et al., 2013; Lepeltier et al., 2014).

Size characterisation of samples was carried out without removing ethanol from the system by evaporation. This is because the transition between ouzo and non-ouzo region is similar with or without solvent evaporation, which has been previously proved (Middha et al., 2019). As for the pH of these samples, it can be expected to be similar due to the small variations in capsaicin concentration and WER.

Table 4.2 Particle size and PDI values of capsaicin nanoparticles obtained using different formulations.

				Size at 0 h		Size at 2 h	
No.	Capsaicin concentration (mg/ml)	Capsaicin solution (µl)	Water (µl)	z-average d (nm)	PDI	z-average d (nm)	PDI
1	1.25	27	273	118 ± 9	0.18	175 ± 5	0.10
2	1.25	39	261	170 ± 17	0.06	254 ± 1	0.06
3	1.25	50	250	256 ± 13	0.06	342 ± 12	0.06
4	2.3	27	273	317 ± 30	0.04	491 ± 6	0.06
5	2.3	39	261	472 ± 47	0.07	645 ± 94	0.14

Characterisation of these formulations has also been conducted replacing water by phosphate buffered saline (PBS buffer) or Dulbecco's Modified Eagle's medium (DMEM) without phenol red in order to test the stability of particles under biological conditions. From Table 4.3, we can see that the size of all samples was relatively larger than those made with water. Higher values of polydispersity were also observed after 2 h. The salt in the PBS could have possibly played a role in the formation of capsaicin nanoparticles. The presence of electrolytes (NaCl, KCl, Na_2HPO_4, KH_2PO_4) in PBS may interfere with the preferential adsorption of –OH ions from water observed in the capsaicin nanoparticles in water. In addition, higher salt concentration could possibly affect system stability, leading to aggregation of nuclei and formation of larger particles. As for the use of DMEM without phenol red instead of water, Table 4.4 showed that the size became even larger and more polydisperse. It seems possible that the components, especially salts, present in the DMEM solution may have disturbed the capsaicin recrystallization process.

Table 4.3 Particle size and PDI values of capsaicin nanoparticles prepared in PBS (salt concentration: ~149.7 mM).

No.	Capsaicin concentration (mg/mL)	Capsaicin solution (µL)	PBS (µL)	Size at 0 h		Size at 2 h	
				z-average d (nm)	PDI	z-average d (nm)	PDI
1	1.25	27	273	219 ± 26	0.03	541 ± 55	0.05
2	1.25	39	261	301 ± 12	0.03	662 ± 20	0.15
3	1.25	50	250	510 ± 22	0.05	587 ± 33	0.57
4	2.3	27	273	596 ± 2	0.12	785 ± 6	1.00
5	2.3	39	261	559 ± 16	0.31	699 ± 6	0.99

Table 4.4 Particle size and PDI values of capsaicin nanoparticles prepared in DMEM (salt concentration: ~165.72 mM).

No.	Capsaicin concentration (mg/mL)	Capsaicin solution (µL)	DMEM (µL)	Size at 0 h		Size at 2 h	
				z-average d (nm)	PDI	z-average d (nm)	PDI
1	1.25	27	273	678 ± 52	0.20	2316 ± 240	0.34
2	1.25	39	261	1619 ± 177	0.11	2646 ± 392	0.55
3	1.25	50	250	1643 ± 348	0.17	2241 ± 713	0.43
4	2.3	27	273	620 ± 36	0.14	649 ± 248	0.89
5	2.3	39	261	1140 ± 29	0.22	1078 ± 146	0.78

4.4 Physicochemical and morphological characterization of nanoemulsions

After the thorough study on the recrystallization of capsaicin, oil was incorporated into the formulations to produce NEs via the solvent displacement method. Size characterization (Table 4.5) shows that, within experimental error, the NEs had rather similar mean droplet size of around 230 nm and PDI < 0.3. Mean size and PDI remained stable up to 24 hours. Though measured using the refractive index of Miglyol®812 instead of capsaicin, these values are kind of similar to size of capsaicin particles without oil. The Zeta potential values determined for these formulations resulted in negative values (ζ= -30 mV), without evident variations for different NEs. The reason for the negative Zeta potential values, given that both Miglyol

monoglycerides and capsaicin are neutral, stems on the preferential adsorption of –OH ions from water. This is a known effect for oil droplets and other colloidal systems (Beattie et al., 2009). The relatively high Zeta potential values are consistent with a moderate stability against aggregation. The little variation in Zeta potential values, is consistent with the notion that the NEs obtained from different conditions all shared very similar surface properties. As for NE produced in same process but without capsaicin the zeta potential value was -39 mV, slightly more negative than those with capsaicin. The pH of these formulations were not measured since the volumes of samples (1-2 mL) were too small for a pH meter. In theory, the pH of these formulations could be similar due to the same capsaicin final concentration.

Table 4.5 Characterisation of nanoemulsions (NEs) with a final capsaicin concentration of ~2.5 mM.

Nanoemulsions No.	Size at Day 0		Size at Day 1		Zeta potential (mV)
	z-average d (nm)	PDI	z-average d (nm)	PDI	
1	263 ± 18	0.35 ± 0.03	229 ±17	0.26 ± 0.02	-33 ± 5
2	221 ± 4	0.24 ± 0.03	212 ± 3	0.18 ± 0.01	-29 ± 5
3	213 ± 4	0.18 ± 0.02	210 ± 8	0.18 ± 0.01	-30 ± 0
4	259 ± 27	0.32 ± 0.03	227 ± 15	0.28 ± 0.06	-32 ± 5
5	246 ± 10	0.25 ± 0.04	220 ± 6	0.21 ± 0.04	-29 ± 0

Note: Different NEs in the table correspond to the conditions and systems shown in Table 4.2, but with different mixing methods.

Among these NEs, No.5 NE was further investigated considering the required volume for biological tests. The tested association efficiency was estimated as 99.5%, meaning nearly all of the capsaicin was deposited in the form of nanoparticles. Transmission electron microscopy (TEM) was used to study the microstructure of the NE produced. TEM images (Figure 4.6) showed spherical particles comprised of sizes ranging from 50 nm to 2 μm. According to the size distribution profile of NE shown in Figure 4.8b, there were a few droplets with size in the range of several microns. Thus, the size of particles from TEM images seemed to agree with DLS measurements. The large particles could be oil droplets, while the smaller population could be either a

second population of oil droplets or capsaicin nanoparticles. However, none of the spherical droplets showed the presence of nanoparticles adsorbed at the interface as it would be expected from Pickering stabilisation.

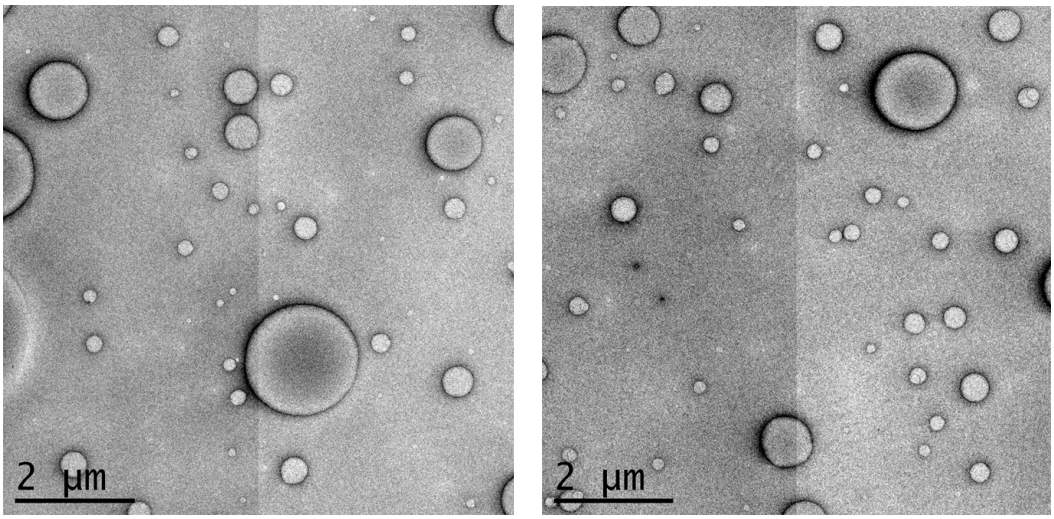

Figure 4.6 TEM images of No.5 NE at the magnification of 2 µm.

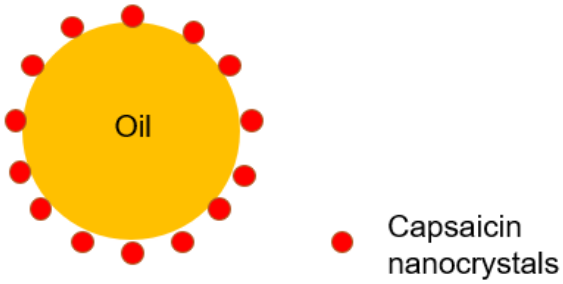

Figure 4.7 Schematic illustration of the Pickering emulsion stabilized by capsaicin nanoparticles.

According to Pickering stabilisation, the expected microstructure of the stable NE should have resembled the one schematically presented in Figure 4.7, in which small capsaicin nanoparticles appear adsorbed at the oil interface. However, the TEM images did not show such clear-cut evidence of Pickering adsorption of nanoparticles at the o/w interface.

We can only offer a highly speculative argumentation to a possible structural alteration of the nanoparticles leading to their detachment from the interface

of NE when preparing the samples for TEM imaging. This could be due to the drying of samples on the grid or the use of slightly radioactive uranyl acetate as a contrast agent. It has been shown that the application of external magnetic or electric fields leads to the detachment of electrically polarizable particles from PE (Hwang et al., 2010).

On a different note, according to requirements for solid particles to serve as effective Pickering stabilizers, one reason to why PE may not have formed, could be the rather large size of capsaicin nanoparticles. Those capsaicin nanoparticles are much larger than surfactant molecules and have slower adsorption dynamics as a result. Usually, the size of the solid particles should be at least one order of magnitude smaller than the PE oil droplets (Ettelaie and Lishchuk, 2015). That means the capsaicin nanoparticles should be smaller than ~20 nm to have achieved Pickering stabilisation. It cannot be ruled out that the large capsaicin nanoparticles observed in the absence of oil, could have suffered a disintegration resulting in a substantial reduction in their particle size during the spontaneous emulsification process. The presence of a dark halo around the NE in the TEM images, may be stem on the existence of a layer of such capsaicin nanoparticles too small to be resolved by TEM imaging at that magnification. Besides, modifications of the capsaicin nanoparticles may help their adsorption. This could be further evaluated by carrying out contact angle measurements that assess the wettability of capsaicin by the oil and water phase.

Another explanation for the system stability could work here is electrostatic stabilization. Because of the preferential adsorption of –OH ions from water, capsaicin nanoparticles and oil droplets dispersed in water are likely stabilized by repulsive electrostatic forces.

Finally, the stability of NE was assessed upon storage at room temperature for 4 days. No cream layer formation or oil layer formation was observed during this period. However, it was observed that the precipitation of needle-like capsaicin crystals (1-2 mm in length) on the second day after formation. This could have been caused by temperature fluctuations at room conditions since recrystallization is very sensitive to temperature change. According to Figure 4.8a, mean average droplet size dropped slightly after the first day and remained stable for consecutive period of study. Figure 4.8b showed the particle size distribution, indicating the good condition of NEs even capsaicin crystals have precipitated. It is crucial to understand how pH and salt concentration changes affect the stability of the formulation, though no further investigation has been done in this term.

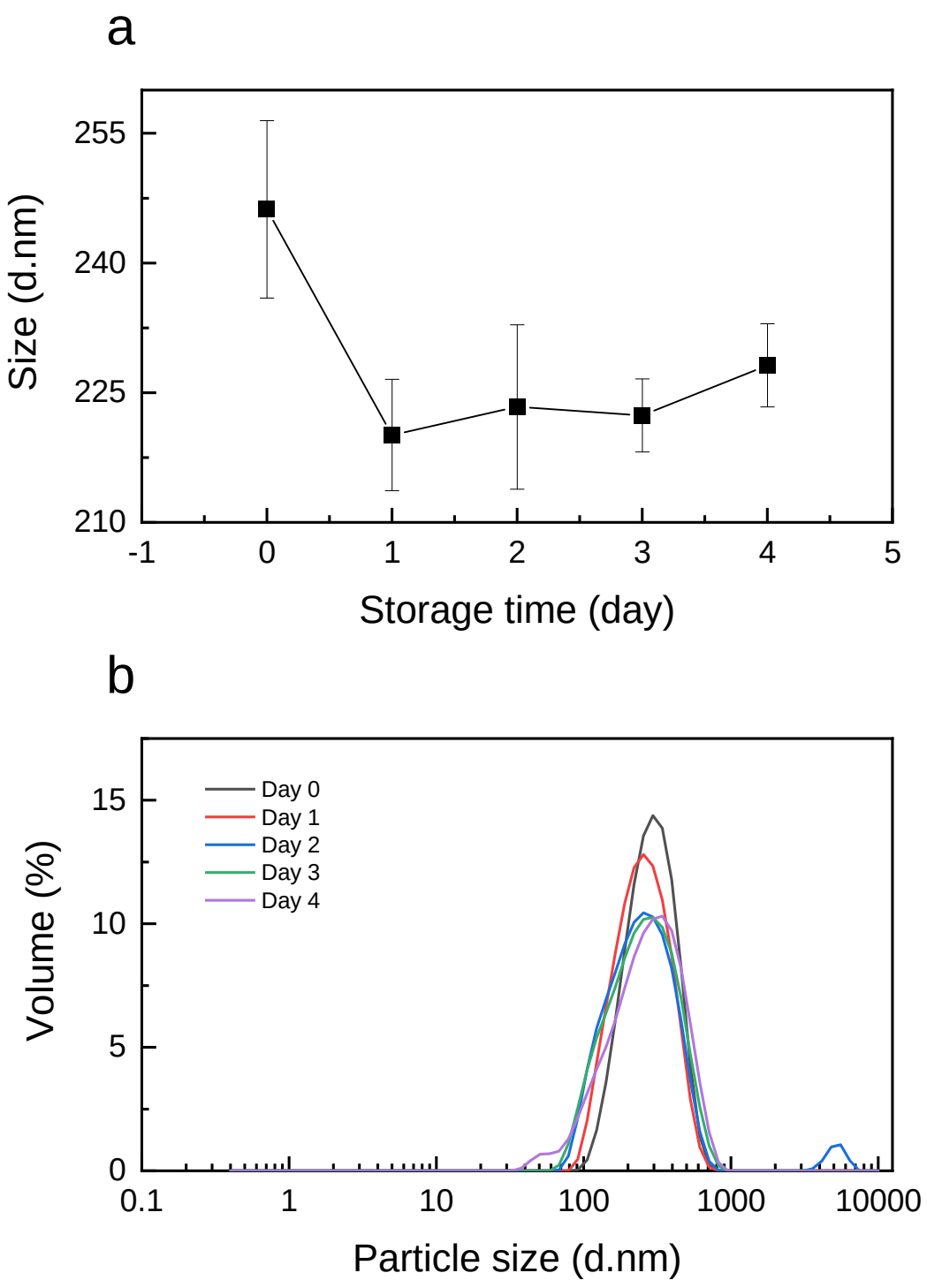

Figure 4.8 The effect of storage time on the mean particle size (a) and the size distribution (b) of capsaicin-loaded nanoemulsion No.5.

4.5 *In vitro* cytotoxicity study

The obtained stable No.5 NE was subsequently examined on its biological activity against MDCK II cells. Cell viability after exposure to chemicals can be assessed by *in vitro* cytotoxicity assays. Conventionally, the MTT assay is used to measure cell metabolic activity under defined conditions. However, this method has drawbacks of being time consuming and labour intensive. According to previous studies (Ceriotti et al., 2007; Lee et al., 2012; Kaiser et al., 2015b), capacitance measurements can be used for real-time and non-invasive assessment of cell viability. Thus, impedance measurements of capacitance were used to investigate cytotoxic effects of different capsaicin-based formulations on MDCK II cell monolayers.

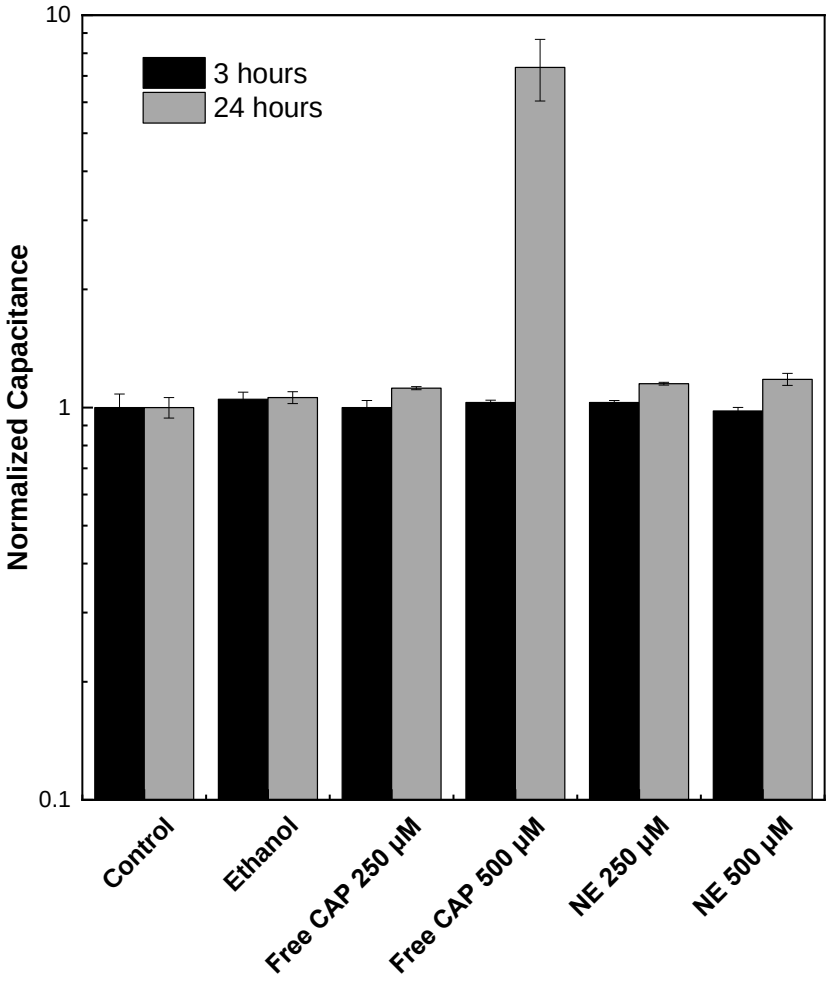

Figure 4.9 Normalized capacitance for cells grown on Transwell inserts with different treatments. The normalized capacitance is relative to the control sample. Measurements were recorded for 3 h and 24 h after applying treatments. Results are average of one biological experiment with at least three technical replicates.

Figure 4.9 shows the values of normalized capacitance estimated at 3 and 24 h after adding treatments. At 3 h, the normalized capacitance for all the treatments was very close to that of the control sample and it increased slightly after 24 h except for the significantly increase observed for 500 µM free capsaicin treatment. This indicated that 500 µM free capsaicin after 24h could cause cell detachment and a significant reduction in cell viability. By contrast, capsaicin-loaded NEs at the same concentration did not induce an increase of capacitance due to cell detachment, revealing a cytoprotective effect on MDCK II cells.

The cytotoxicity of capsaicin has been investigated in many kind of cells. This effect depends on time of exposure and concentration. For epithelial cell lines including MDCK-C7 cells (Kaiser et al., 2015b), Caco-2 cells (Kaiser et al., 2017; Tsukura et al., 2007) and TR146 cells (Kaiser et al., 2015a), it is reported that a strong reduction of cell viability would happen at doses higher than 300 µM as determined by MTT assay. As for impedance measurements, previous research has shown the capacitance of MDCK-C7 cells increased significantly after 24 h by 750 µM. Considering their different cultivated surface areas, the results from two methods were consistent. Free capsaicin has been shown to be more toxic towards MDCK II cells, compared to results of capacitance measurements obtained for MDCK-C7 cells.

The reason for the cytotoxic effect shown by capsaicin is that capsaicin can induce an inhibition of cell proliferation and evoke apoptosis. This is possibly related to an increase in intracellular calcium influx, generation of reactive oxygen species, disruption of inner mitochondrial membrane potential and activation of some transcription factors in many malignant cells (Maksimova et al., 2016). It has also been shown that the cytotoxic effect of capsaicin works similar to the normal counterpart as well (Helvaci and Cömertpay, 2018). This may explain the observed cytotoxicity of capsaicin in MDCK type II cells.

The obtained results should be confirmed with further biological replicates.

4.6 Cell permeability study

To study the permeability of MDCK II cells and the integrity of tight junctions under capsaicin exposure, automated impedance measurements of TEER were carried out. Figure 4.10 shows the evolution of relative TEER response of MDCK monolayers to different treatments. It is clear that capsaicin induces

a reversible decrease in TEER. The effect of capsaicin on the tight junctions was dose-dependent and the capsaicin-loaded NEs were shown to modulate the reversible disruption of the tight junctions.

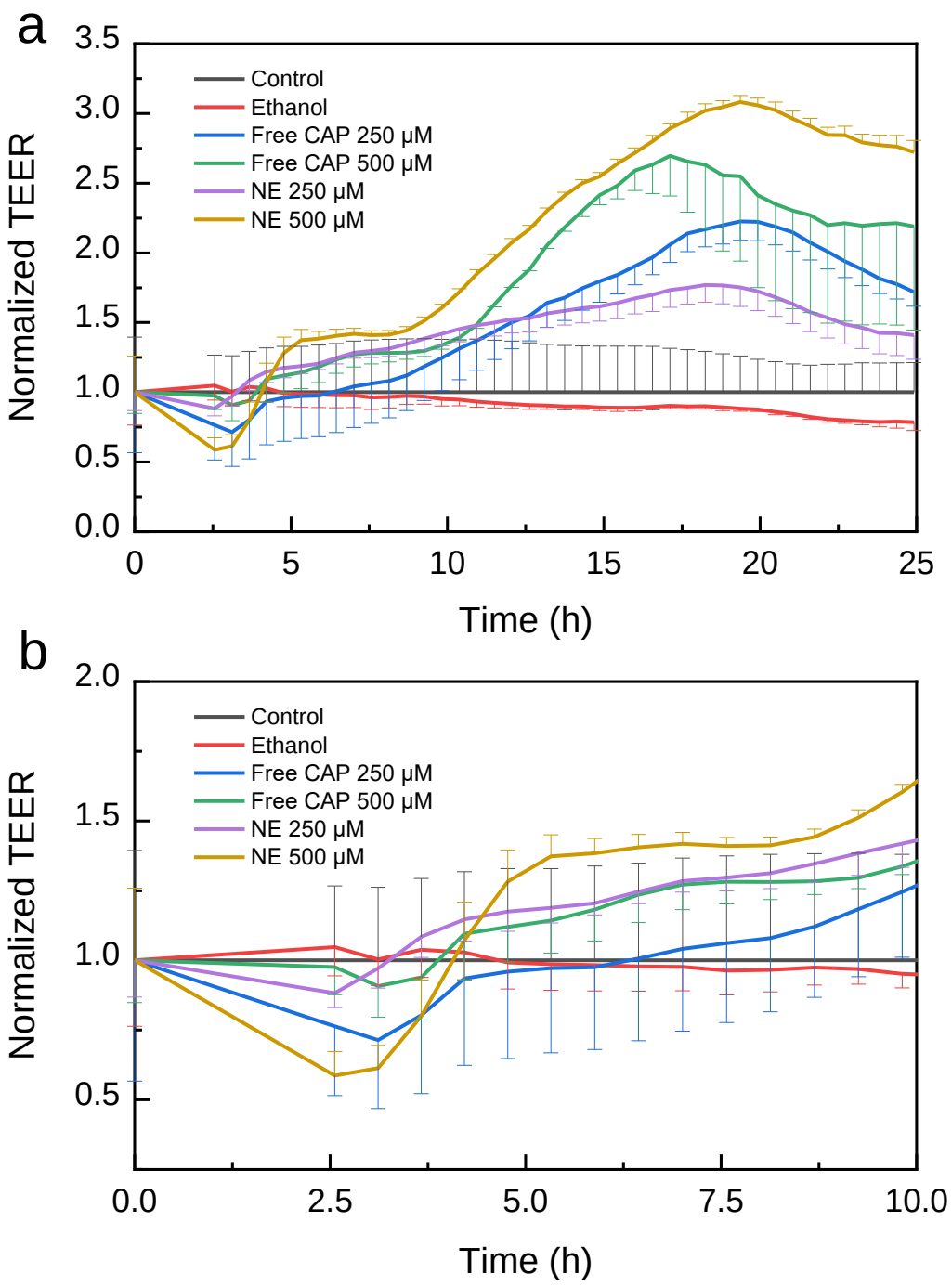

Figure 4.10 Time course of normalized TEER relative to the control with different treatments. (a) The TEER values over 24 hours. (b) An insight of TEER reduction. Results are average of one biological experiment with at least three technical replicates. CAP: capsaicin.

Compared to the control and ethanol, free and emulsified capsaicin induced a decrease in TEER values of MDCK II cell monolayers at the very beginning and recovered to the initial value without removal of capsaicin. Surprisingly, a doubling the dose of free capsaicin from 250 to 500 µM induced a smaller TEER reduction (< 10%). On the contrary, for capsaicin-loaded NEs, doubling the dose of capsaicin resulted in a more pronounced TEER decrease, down to ~60% at ~2.5 h of the original value for NE with 500 µM of capsaicin. After the early reductions, the TEER values recovered in both free capsaicin and capsaicin-loaded NEs, but with notorious differences in the recovery time, following the order: free CAP 250 µM > NE 500 µM = free CAP 500 µM > NE 250 µM. Beyond recovery, all treatments resulted in an increase in TEER values from the original ones. And then the TEER values decreased in this order: NE 500 µM >> free CAP 500 µM > free CAP 250 µM > NE 250 µM. When reaching end-point values (25 h), NE with 500 µM capsaicin increased to up to 150% of the original values.

Previous studies have demonstrated the capsaicin–induced reversible decrease in TEER in Caco-2 cells (Han, J.K. et al., 2005), MDCK-C7 cells (Kaiser et al., 2015b) and even MDCK type II cells (Shiobara et al., 2013). It was shown that the effect of capsaicin on the TEER of MDCK II monolayers was dose dependent, with TEER almost unchanged at 30 µM capsaicin, but significantly reduced to around 50% after 2 h when 100 and 300 µM capsaicin were applied. Those observations are slightly different from what it was observed in this study, in which not only TEER was capsaicin dose dependent but also the degree of variation, was unexpected. The reason for this may have been related to the preparation of the free capsaicin solution. Capsaicin was firstly dissolved in ethanol and then diluted by large amount of DMEM before being applied to cells. As mentioned before, capsaicin was seen to be extremely unstable in DMEM. Mixing these by pipetting could have led to the formation of large particles. Thus, the TEER results could have been affected by the preparation protocol. However, the capsaicin-based NEs were more stable when diluted and displayed a dose dependent pattern as expected.

As for the duration of tight junction opening, it is not very clear since there is a time lag at the very beginning because of treatments addition. However, it can be roughly inferred from the graph that it could have taken up to 2 – 6 h for TEER to recover. Previous studies indicated that tight junction opening lasted for ~6 h for MDCK II cells when treated with 300 µM (Shiobara et al., 2013), which is close to our estimation. For MDCK-C7 cells, longer times (12.5 - 24 h) were required to close tight junctions (Kaiser et al., 2015b). The

difference in duration of tight junction opening could be probably related to the different biological properties of different cell strains. Although they are both from the parental MDCK cells, MDCK-C7 cells are isolated from lower passages and have very tight junctions with high TEER values of more than 4000 Ω•cm^2, while MDCK II cells used in the present study are from higher passages and hence, display lower TEER (less than 300 Ω•cm^2), diagnostic of leaky junctions. This is due to the difference in the composition of tight junction as the expression of tight junction protein claudin-2 in MDCK type II cells (Dukes et al., 2011). For very tight junctions, it is possible that longer time of exposure is required for opening. However, a quick tight junction opening is desirable since it would ensure the proper function of the barrier, avoiding the entry of metabolic waste as well as the leakage of important proteins and nutrients. Therefore, a given drug can be safely co-delivered and controllably absorbed.

Previous studies indicated that capsaicin in the form of nanoemulsions and nanocapsules could modulate the tight junction opening. If compared to the decrease effect induced by 100 and 300 µM capsaicin in previous study (Shiobara et al., 2013), the NE in our study could also attenuate the effect. It seemed capsaicin in the form of nanoparticles would attenuate its cytotoxicity as well as the tight junction opening. Whether it can reduce its pungency remains to be determined.

After reversible tight junction opening (5 h), the TEER values kept increasing and exceeded the initial values by up to 3-fold, indicating that monolayers become tighter under the effect of capsaicin. It seems that capsaicin can also reorganize and strengthen the structure of epithelial tight junctions after recovery. Previous study has reported that capsaicin derivatives (e.g. dihydrocapsaicin, nonivamide) that displaying reversible opening of tight junctions recovered to a higher value than initial (Kaiser et al., 2016a). However, no study has reported this for capsaicin.

Chapter 5
Conclusions

5.1 Summary

In this work, the ouzo region for the formation of capsaicin nanoparticles in mixtures of ethanol/water was identified in the ternary phase diagram. To our knowledge, this is the first report of the ouzo effect of capsaicin. The size of capsaicin nanoparticles can be controlled in size ranging from ~100 to ~500 nm by the increase of capsaicin mass fraction. Introducing of oil into the system produced a stable o/w NE using the solvent displacement method. This is a simple, surfactant-free and low-energy protocol. In this case (using different mixing method), the size of capsaicin nanoparticles can be substantially reduced to around 50 nm or even smaller that is not seen at that magnification, while the size of oil droplets is around 200 nm. However, contrary to our hypothesis, at this stage, we cannot conclude unequivocally that the mechanism of stabilization is due to Pickering adsorption of capsaicin nanoparticles or a different, yet to elucidate, phenomenon. The obtained formulations seem to be sensitive to temperature not only in the process but also during the storage. As for the biological effect, the obtained NE formulation was found to attenuate the toxicity of capsaicin and to have a pronounced effect on tight junction opening when applied to a model epithelial monolayer of MDCK II cells. In addition, the effect of tight junction opening lasts for shorter times than when cells are exposed to free capsaicin. Overall, these results suggest that the NE produced here is a safer and more robust option for the modulation of tight junctions permeability. It may offer a novel strategy for the delivery of large and hydrophilic molecules through paracellular pathway.

5.2 Future work

Validation of solubility tests and impedance measurements can provide confirmation of these preliminary results. Though labor-intensive, the tetrazolium-based MTT assay should be carried out for the formulations produced here to assess their cytotoxicity as it is a highly sensitive method and a standard protocol. It is also worthwhile to test whether this type of NE modulates the pungency of capsaicin in its present form as nanoparticles.

Further studies utilizing more advanced methods (e.g. aggregation-induced dye emission) can provide more information about the ouzo region of capsaicin in the ternary phase diagram. In addition, extra tests can be performed by adding salt to the system to see if the stabilization mechanism is electrostatic repulsion due to adsorption of some charge species in the surface of droplets.

It also remains to be determined why capsaicin nanoparticles do not adsorb at the interface and assess if Pickering emulsions using capsaicin nanoparticles could be formed using high shear technologies. Further investigations are recommended for the evaluation of the wettability of capsaicin nanoparticles in terms of contact angle, which should give an insight of the interface adsorption efficiency. Modifications in size, surface charge and concentration may help capsaicin nanoparticles to adsorb at the interface. Techniques able to offer atomic resolution such as small-angle X-ray scattering (SAXS) may help to elucidate the nature of the o/w interface of the capsaicin-stabilized NEs.

List of References

Aditya, N.P., Hamilton, I.E. and Norton, I.T. 2017. Amorphous nano-curcumin stabilized oil in water emulsion: Physico chemical characterization. *Food Chemistry.* **224**, pp.191-200.

Albert, C., Beladjine, M., Tsapis, N., Fattal, E., Agnely, F. and Huang, N. 2019. Pickering emulsions: Preparation processes, key parameters governing their properties and potential for pharmaceutical applications. *Journal of Controlled Release.* **309**, pp.302-332.

Amidon, G.L., Lennernäs, H., Shah, V.P. and Crison, J.R. 1995. A Theoretical Basis for a Biopharmaceutic Drug Classification: The Correlation of in Vitro Drug Product Dissolution and in Vivo Bioavailability. *Pharmaceutical Research.* **12**(3), pp.413-420.

Anton, N. and Vandamme, T.F. 2011. Nano-emulsions and Micro-emulsions: Clarifications of the Critical Differences. *Pharmaceutical Research.* **28**(5), pp.978-985.

Aschenbrenner, E., Bley, K., Koynov, K., Makowski, M., Kappl, M., Landfester, K. and Weiss, C.K. 2013. Using the Polymeric Ouzo Effect for the Preparation of Polysaccharide-Based Nanoparticles. *Langmuir.* **29**(28), pp.8845-8855.

Aungst, B.J. 2012. Absorption Enhancers: Applications and Advances. *The AAPS journal.* **14**(1), pp.10-18.

Beattie, J.K., Djerdjev, A.M. and Warr, G.G. 2009. The surface of neat water is basic. *Faraday Discuss.* **141**, pp.31-39; discussion 81-98.

Beck-Broichsitter, M., Rytting, E., Lebhardt, T., Wang, X. and Kissel, T. 2010. Preparation of nanoparticles by solvent displacement for drug delivery: A shift in the "ouzo region" upon drug loading. *European Journal of Pharmaceutical Sciences.* **41**(2), pp.244-253.

Benson, K., Cramer, S. and Galla, H.J. 2013. Impedance-based cell monitoring: barrier properties and beyond. *Fluids Barriers CNS.* **10**(1), p5.

Bocsik, A., Walter, F.R., Gyebrovszki, A., Fülöp, L., Blasig, I., Dabrowski, S., Ötvös, F., Tóth, A., Rákhely, G., Veszelka, S., Vastag, M., Szabó-Révész, P. and Deli, M.A. 2016. Reversible Opening of Intercellular Junctions of Intestinal Epithelial and Brain Endothelial Cells With Tight Junction Modulator Peptides. *Journal of pharmaceutical sciences.* **105**(2), pp.754-765.

Bonnett, P., Carpenter, K., Dawson, S. and Davey, R.J.C.c. 2003. Solution crystallisation via a submerged liquid–liquid phase boundary: oiling out. *Chemical Communications.* (6), pp.698-699.

Botet, R. 2012. The "ouzo effect", recent developments and application to therapeutic drug carrying. *Journal of Physics: Conference Series.* **352**, p012047.

Cayman Chemical. 2020. *Product information.* [Online]. [Accessed February 23, 2021]. Available from: https://www.caymanchem.com/pdfs/92350.pdf

Ceriotti, L., Ponti, J., Broggi, F., Kob, A., Drechsler, S., Thedinga, E., Colpo, P., Sabbioni, E., Ehret, R. and Rossi, F. 2007. Real-time assessment of cytotoxicity by impedance measurement on a 96-well plate. *Sensors and Actuators B: Chemical.* **123**(2), pp.769-778.

Chen, L., Ao, F., Ge, X. and Shen, W. 2020. Food-Grade Pickering Emulsions: Preparation, Stabilization and Applications. *Molecules (Basel, Switzerland).* **25**(14), p3202.

Cho, S.-C., Lee, H. and Choi, B.Y. 2017. An updated review on molecular mechanisms underlying the anticancer effects of capsaicin. *Food science and biotechnology.* **26**(1), pp.1-13.

Clark, R. and Lee, S.H. 2016. Anticancer Properties of Capsaicin Against Human Cancer. *Anticancer Research.* **36**(3), p837.

Costanzo, M.T., Yost, R.A. and Davenport, P.W. 2014. Standardized method for solubility and storage of capsaicin-based solutions for cough induction. *Cough (London, England).* **10**(1), pp.6-6.

Deli, M.A. 2009. Potential use of tight junction modulators to reversibly open membranous barriers and improve drug delivery. *Biochimica et Biophysica Acta (BBA) - Biomembranes.* **1788**(4), pp.892-910.

Din, F.U., Aman, W., Ullah, I., Qureshi, O.S., Mustapha, O., Shafique, S. and Zeb, A. 2017. Effective use of nanocarriers as drug delivery systems for the treatment of selected tumors. *International journal of nanomedicine.* **12**, pp.7291-7309.

Du, Q., Liao, Q., Chen, C., Yang, X., Xie, R. and Xu, J. 2019. The Role of Transient Receptor Potential Vanilloid 1 in Common Diseases of the Digestive Tract and the Cardiovascular and Respiratory System. **10**(1064).

Dukes, J.D., Whitley, P. and Chalmers, A.D. 2011. The MDCK variety pack: choosing the right strain. *BMC cell biology.* **12**, pp.43-43.

El-Kaaby, E., Al Hattab, Z. and A, A.-A. 2016. FT-IR Identification of Capsaicin from callus and seedling of chilli pepper plants Capsicum annuum L. in vitro. *International Journal of Multidisciplinary and Current Research* **4**, pp.1144-1146.

Ettelaie, R. and Lishchuk, S.V. 2015. Detachment force of particles from fluid droplets.

Fattori, V., Hohmann, M., Rossaneis, A., Pinho-Ribeiro, F. and Verri, W. 2016. Capsaicin: Current Understanding of Its Mechanisms and Therapy of Pain and Other Pre-Clinical and Clinical Uses. *Molecules.* **21**(7), p844.

Fessi, H., Puisieux, F., Devissaguet, J.P., Ammoury, N. and Benita, S. 1989. Nanocapsule formation by interfacial polymer deposition following solvent displacement. *International Journal of Pharmaceutics.* **55**(1), pp.R1-R4.

François, G. and Katz, J.L. 2005. Nanoparticles and nanocapsules created using the Ouzo effect: spontaneous emulisification as an alternative to ultrasonic and high-shear devices. *Chemphyschem.* **6**(2), pp.209-216.

Galindo-Rodriguez, S., Allémann, E., Fessi, H. and Doelker, E. 2004. Physicochemical Parameters Associated with Nanoparticle Formation in the Salting-Out, Emulsification-Diffusion, and Nanoprecipitation Methods. *Pharmaceutical Research.* **21**(8), pp.1428-1439.

Giri, T.K., Mukherjee, P., Barman, T.K. and Maity, S. 2016. Nano-encapsulation of capsaicin on lipid vesicle and evaluation of their hepatocellular protective effect. *International Journal of Biological Macromolecules.* **88**, pp.236-243.

Gv, S., Daniel, D., Kv, S. and Krk, M. 2018. An Alternate Solvent for the Determination of Capsaicin Content in Chillies by HPLC Method. *Natural Products Chemistry & Research.* **06**.

Han, J.K., Akutsu, M., Talorete, T.P.N., Maekawa, T., Tanaka, T. and Isoda, H. 2005. Capsaicin-enhanced ribosomal protein P2 expression in human intestinal Caco-2 cells. *Cytotechnology.* **47**(1-3), pp.89-96.

Han, J.Y., Isoda, H. and Maekawa, T. 2002. Analysis of the mechanism of the tight-junctional permeability increase by capsaicin treatment on the intestinal Caco-2 cells. *Cytotechnology.* **40**(1-3), pp.93-98.

Helvaci, N. and Cömertpay, S. 2018. In vitro evaluation of the effects of capsaicin on normal and cancerous cells of human cartilage. *Turkish journal of biology.* **42**(5), pp.422-434.
Homayun, B., Lin, X. and Choi, H.-J. 2019. Challenges and Recent Progress in Oral Drug Delivery Systems for Biopharmaceuticals. *Pharmaceutics.* **11**(3), p129.
Hunter, T.N., Pugh, R.J., Franks, G.V. and Jameson, G.J. 2008. The role of particles in stabilising foams and emulsions. *Advances in Colloid and Interface Science.* **137**(2), pp.57-81.
Hwang, K., Singh, P. and Aubry, N. 2010. Destabilization of Pickering emulsions using external electric fields. *Electrophoresis.* **31**(5), pp.850-859.
Ibrahim, Y.H.E.Y., Regdon, G., Hamedelniel, E.I. and Sovány, T. 2020. Review of recently used techniques and materials to improve the efficiency of orally administered proteins/peptides. *Journal of Pharmaceutical Sciences.* **28**(1), pp.403-416.
Jara-Oseguera, A., Simon, S.A. and Rosenbaum, T. 2008. TRPV1: on the road to pain relief. *Current molecular pharmacology.* **1**(3), pp.255-269.
Johnson, L.G. 2005. Applications of imaging techniques to studies of epithelial tight junctions. *Advanced Drug Delivery Reviews.* **57**(1), pp.111-121.
Jovov, B., Wills, N.K. and Lewis, S.A. 1991. A spectroscopic method for assessing confluence of epithelial cell cultures. *Am J Physiol.* **261**(6 Pt 1), pp.C1196-1203.
Juturu, V. 2016. Capsaicinoids Modulating Cardiometabolic Syndrome Risk Factors: Current Perspectives. *Journal of Nutrition and Metabolism.* **2016**, p4986937.
Kaiser, M., Burek, M., Britz, S., Lankamp, F., Ketelhut, S., Kemper, B., Forster, C., Gorzelanny, C. and Goycoolea, F.M. 2019. The Influence of Capsaicin on the Integrity of Microvascular Endothelial Cell Monolayers. *International Journal of Molecular Sciences.* **20**(1), p122.
Kaiser, M., Chalapala, S., Gorzelanny, C., Perali, R.S. and Goycoolea, F.M. 2016a. The Effect of Capsaicin Derivatives on Tight-Junction Integrity and Permeability of Madin-Darby Canine Kidney Cells. *Journal of pharmaceutical sciences.* **105**(2), pp.630-638.
Kaiser, M., Higuera, I. and Goycoolea, F.M. 2017. Capsaicinoids: Occurrence, Chemistry, Biosynthesis, and Biological Effects. *Fruit and Vegetable Phytochemicals: Chemistry and Human Health, 2nd Edition.* pp.499-514.
Kaiser, M., Kirsch, B., Hauser, H., Schneider, D., Seuss-Baum, I. and Goycoolea, F.M. 2015a. In Vitro and Sensory Evaluation of Capsaicin-Loaded Nanoformulations. *PLoS One.* **10**(10), pe0141017.
Kaiser, M., Lankamp, F. and Goycoolea, F.M. 2016b. Nanoencapsulation of Capsaicin Attenuates the Cytotoxic Effect on Caco-2 Cells. *Gums and Stabilisers for the Food Industry 18: Hydrocolloid Functionality for Affordable and Sustainable Global Food Solutions.* The Royal Society of Chemistry, pp.176-181.
Kaiser, M., Pereira, S., Pohl, L., Ketelhut, S., Kemper, B., Gorzelanny, C., Galla, H.J., Moerschbacher, B.M. and Goycoolea, F.M. 2015b. Chitosan encapsulation modulates the effect of capsaicin on the tight junctions of MDCK cells. *Scientific Reports.* **5**, p10048.
Kiptoo, P., Calcagno, A.M. and Siahaan, T.J. 2016. Physiological, Biochemical, and Chemical Barriers to Oral Drug Delivery. *Drug Delivery.* pp.19-34.
Kobata, K., Todo, T., Yazawa, S., Iwai, K. and Watanabe, T. 1998. Novel Capsaicinoid-like Substances, Capsiate and Dihydrocapsiate, from the Fruits of a Nonpungent

Cultivar, CH-19 Sweet, of Pepper (Capsicum annuum L.). *Journal of Agricultural and Food Chemistry.* **46**(5), pp.1695-1697.
Kometani, T., Tanimoto, H., Nishimura, T., Kanbara, I. and Okada, S. 1993. Glucosylation of Capsaicin by Cell Suspension Cultures of Coffea arabica. *Bioscience, Biotechnology, and Biochemistry.* **57**(12), pp.2192-2193.
Koroleva, M.Y. and Yurtov, E.V. 2012. Nanoemulsions: the properties, methods of preparation and promising applications. *Russian Chemical Reviews.* **81**(1), pp.21-43.
Krug, S.M., Fromm, M. and Günzel, D. 2009. Two-path impedance spectroscopy for measuring paracellular and transcellular epithelial resistance. *Biophysical journal.* **97**(8), pp.2202-2211.
Kulkarni, Y.A., Suryavanshi, S.V., Auti, S.T. and Gaikwad, A.B. 2017. Chapter 9 - Capsicum: A Natural Pain Modulator. In: Watson, R.R. and Zibadi, S. eds. *Nutritional Modulators of Pain in the Aging Population.* Academic Press, pp.107-119.
Kumar, V. and Prud'homme, R.K. 2009. Nanoparticle stability: Processing pathways for solvent removal. *Chemical Engineering Science.* **64**(6), pp.1358-1361.
Lachman, L., Lieberman, H.A. and Kanig, J.L. 1986. *The theory and practice of industrial pharmacy.* Lea & Febiger.
Lea, T. 2015. Epithelial cell models; general introduction. *The Impact of Food Bioactives on Health.* Springer International Publishing, pp.95-102.
Lee, R., Kim, J., Kim, S.Y., Jang, S.M., Lee, S.M., Choi, I.H., Park, S.W., Shin, J.S. and Yoo, K.H. 2012. Capacitance-based assay for real-time monitoring of endocytosis and cell viability. *Lab Chip.* **12**(13), pp.2377-2384.
Lepeltier, E., Bourgaux, C. and Couvreur, P. 2014. Nanoprecipitation and the "Ouzo effect": Application to drug delivery devices. *Advanced drug delivery reviews.* **71**, pp.86-97.
Linke, C. and Drusch, S. 2018. Pickering emulsions in foods - opportunities and limitations. *Critical Reviews in Food Science and Nutrition.* **58**(12), pp.1971-1985.
Lu, M., Chen, C., Lan, Y., Xiao, J., Li, R., Huang, J., Huang, Q., Cao, Y. and Ho, C.-T. 2020. Capsaicin-the major bioactive ingredient of chili peppers: bio-efficacy and delivery systems. *Food & function.* **11**(4), pp.2848-2286.
Luongo, L., Costa, B., D'Agostino, B., Guida, F., Comelli, F., Gatta, L., Matteis, M., Sullo, N., De Petrocellis, L., de Novellis, V., Maione, S. and Di Marzo, V. 2012. Palvanil, a non-pungent capsaicin analogue, inhibits inflammatory and neuropathic pain with little effects on bronchopulmonary function and body temperature. *Pharmacological Research.* **66**(3), pp.243-250.
Maksimova, V., Gudeva, L.K., Gulaboski, R. and Nieber, K. 2016. Co-extracted bioactive compounds in Capsicum fruit extracts prevent the cytotoxic effects of capsaicin on B104 neuroblastoma cells. *Revista Brasileira de Farmacognosia.* **26**(6), pp.744-750.
Markov, A.G., Kruglova, N.M., Fomina, Y.A., Fromm, M. and Amasheh, S. 2012. Altered expression of tight junction proteins in mammary epithelium after discontinued suckling in mice. *Pflugers Archiv : European journal of physiology.* **463**(2), pp.391-398.
McClements, D.J. 2021. Advances in edible nanoemulsions: Digestion, bioavailability, and potential toxicity. *Progress in Lipid Research.* **81**, p101081.
Meng, Z., Huang, Y., Cheng, S. and Wang, J. 2020. Investigation of Oiling-Out Phenomenon of Small Organic Molecules in Crystallization Processes: A Review. *ChemistrySelect.* **5**(26), pp.7855-7866.

Middha, E., Manghnani, P., Ng, D., Chen, H., Khan, S. and Liu, B. 2019. Direct Visualization of Ouzo Zone through Aggregation-Induced Emission Dye for the Synthesis of Highly Monodispersed Polymeric Nanoparticles. *Materials Chemistry Frontiers.* **3**.

Monégier du Sorbier, Q., Aimable, A. and Pagnoux, C. 2015. Influence of the electrostatic interactions in a Pickering emulsion polymerization for the synthesis of silica–polystyrene hybrid nanoparticles. *Journal of Colloid and Interface Science.* **448**, pp.306-314.

Mukaiyama, M., Yamasaki, Y., Usui, T. and Nagumo, Y. 2019. Transient receptor potential V4 channel stimulation induces reversible epithelial cell permeability in MDCK cell monolayers. *FEBS letters.* **593**(16), pp.2250-2260.

National Pain Centers. 2019. *Routes of Administration.* [Online]. [Accessed February 17, 2021]. Available from: http://www.nationalpain.com/routes-of-administration

Niessen, C.M. 2007. Tight Junctions/Adherens Junctions: Basic Structure and Function. *Journal of Investigative Dermatology.* **127**(11), pp.2525-2532.

Ortiz, D.G., Pochat-Bohatier, C., Cambedouzou, J., Bechelany, M. and Miele, P. 2020. Current Trends in Pickering Emulsions: Particle Morphology and Applications. *Engineering.* **6**(4), pp.468-482.

Patel, R.B., Patel, M.R., Thakore, S.D. and Patel, B.G. 2017. Chapter 17 - Nanoemulsion as a Valuable Nanostructure Platform for Pharmaceutical Drug Delivery. In: Grumezescu, A.M. ed. *Nano- and Microscale Drug Delivery Systems.* Elsevier, pp.321-341.

Salama, N.N., Eddington, N.D. and Fasano, A. 2006. Tight junction modulation and its relationship to drug delivery. *Tight junctions.* Springer, pp.206-219.

Schneeberger, E.E. and Lynch, R.D. 2004. The tight junction: a multifunctional complex. *Am J Physiol Cell Physiol.* **286**(6), pp.C1213-1228.

Scoville, W.L. 1912. Note on Capsicums. *The Journal of the American Pharmaceutical Association (1912).* **1**(5), pp.453-454.

Shaker, D.S., Ishak, R.A., Ghoneim, A. and Elhuoni, M.A.J.S.P. 2019. Nanoemulsion: A Review on Mechanisms for the Transdermal Delivery of Hydrophobic and Hydrophilic Drugs. *Sci. Pharm.* **87**(3), p17.

Sharma, M., Sharma, R. and Jain, D.K. 2016. Nanotechnology Based Approaches for Enhancing Oral Bioavailability of Poorly Water Soluble Antihypertensive Drugs. *Scientifica.* **2016**, p8525679.

Sheller, R.A., Cuevas, M.E. and Todd, M.C. 2017. Comparison of transepithelial resistance measurement techniques: Chopsticks vs. Endohm. *Biological Procedures Online.* **19**(1), p4.

Shiobara, T., Usui, T., Han, J., Isoda, H. and Nagumo, Y. 2013. The Reversible Increase in Tight Junction Permeability Induced by Capsaicin Is Mediated via Cofilin-Actin Cytoskeletal Dynamics and Decreased Level of Occludin. *Plos One.* **8**(11).

Smutzer, G. and Devassy, R.K. 2016. Integrating TRPV1 Receptor Function with Capsaicin Psychophysics. *Advances in Pharmacological Sciences.* **2016**, p1512457.

Solans, C., Morales, D. and Homs, M. 2016. Spontaneous emulsification. *Current Opinion in Colloid & Interface Science.* **22**, pp.88-93.

Srinivasan, B., Kolli, A.R., Esch, M.B., Abaci, H.E., Shuler, M.L. and Hickman, J.J. 2015. TEER measurement techniques for in vitro barrier model systems. *Journal of laboratory automation.* **20**(2), pp.107-126.

Steed, E., Rodrigues, N.T.L., Balda, M.S. and Matter, K. 2009. Identification of MarvelD3 as a tight junction-associated transmembrane protein of the occludin family. *BMC Cell Biology.* **10**(1), p95.

Sun, M., Du, S., Chen, M., Rohani, S., Zhang, H., Liu, Y., Sun, P., Wang, Y., Shi, P., Xu, S. and Gong, J. 2018. Oiling-Out Investigation and Morphology Control of β-Alanine Based on Ternary Phase Diagrams. *Crystal Growth & Design.* **18**(2), pp.818-826.

Svenson, S. 2004. Carrier-Based Drug Delivery. *Carrier-Based Drug Delivery.* American Chemical Society, pp.2-23.

Takasuga, M. and Ooshima, H. 2014. Control of Crystal Size during Oiling Out Crystallization of an API. *Crystal Growth & Design.* **14**(11), pp.6006-6011.

Tominaga, M. and Tominaga, T. 2005. Structure and function of TRPV1. *Pflügers Archiv.* **451**(1), pp.143-150.

Tran, T.-T. and Hadinoto, K. 2017. A new solubility enhancement strategy of capsaicin in the form of high-payload submicron capsaicin-chitosan colloidal complex. *Colloids and Surfaces A: Physicochemical and Engineering Aspects.* **520**, pp.62-71.

Tsavas, P., Polydorou, S., Voutsas, E.C., Magoulas, K.G., Naraghi, K. and Halling, P.J. 2002. Sucrose Solubility in Mixtures of Water, Alcohol, Ester, and Acid. *Journal of Chemical & Engineering Data.* **47**(3), pp.513-517.

Tsukita, S., Furuse, M. and Itoh, M. 2001. Multifunctional strands in tight junctions. *Molecular Cell Biology.* **2**(4), pp.285-293.

Tsukura, Y., Mori, M., Hirotani, Y., Ikeda, K., Amano, F., Kato, R., Ijiri, Y. and Tanaka, K. 2007. Effects of capsaicin on cellular damage and monolayer permeability in human intestinal Caco-2 cells. *Biological & Pharmaceutical Bulletin.* **30**(10), pp.1982-1986.

Valim, T.C., Cunha, D.A., Francisco, C.S., Romão, W., Filgueiras, P.R., Bezerra dos Santos, R., Borges, W.d.S., Conti, R., Lacerda, V. and Neto, A.C. 2019. Quantification of capsaicinoids from chili peppers using 1H NMR without deuterated solvent. *Analytical Methods.* **11**(14), pp.1939-1950.

Vermette, D., Hu, P., Canarie, M.F., Funaro, M., Glover, J. and Pierce, R.W. 2018. Tight junction structure, function, and assessment in the critically ill: a systematic review. *Intensive Care Medicine Experimental.* **6**(1), p37.

Vitale, S.A. and Katz, J.L. 2003. Liquid Droplet Dispersions Formed by Homogeneous Liquid−Liquid Nucleation: "The Ouzo Effect". *Langmuir.* **19**(10), pp.4105-4110.

Weber, C.R. 2012. Dynamic properties of the tight junction barrier. *Annals of the New York academy of sciences.* **1257**, p77.

Whitby, C.P. and Wanless, E.J. 2016. Controlling Pickering Emulsion Destabilisation: A Route to Fabricating New Materials by Phase Inversion. *Materials (Basel, Switzerland).* **9**(8), p626.

Yan, H., Wang, Z. and Wang, J. 2012. Correlation of Solubility and Prediction of the Mixing Properties of Capsaicin in Different Pure Solvents. *Industrial & Engineering Chemistry Research.* **51**(6), pp.2808-2813.

Yang, F. and Zheng, J. 2017. Understand spiciness: mechanism of TRPV1 channel activation by capsaicin. *Protein & cell.* **8**(3), pp.169-177.

Yang, Y., Fang, Z., Chen, X., Zhang, W., Xie, Y., Chen, Y., Liu, Z. and Yuan, W. 2017. An Overview of Pickering Emulsions: Solid-Particle Materials, Classification, Morphology, and Applications. **8**(287).

Ye, C. and Chi, H. 2018. A review of recent progress in drug and protein encapsulation: Approaches, applications and challenges. *Materials Science and Engineering: C.* **83**, pp.233-246.

Yeh, T.H., Hsu, L.W., Tseng, M.T., Lee, P.L., Sonjae, K., Ho, Y.C. and Sung, H.W. 2011. Mechanism and consequence of chitosan-mediated reversible epithelial tight junction opening. *Biomaterials.* **32**(26), pp.6164-6173.

Zembyla, M., Murray, B.S. and Sarkar, A. 2020. Water-in-oil emulsions stabilized by surfactants, biopolymers and/or particles: a review. *Trends in Food Science & Technology.* **104**, pp.49-59.

Zhang, L., Wang, S., Zhang, M. and Sun, J. 2013. Nanocarriers for oral drug delivery. *Journal of Drug Targeting.* **21**(6), pp.515-527.

Zhang, X.H., Wei, Z.X., Choi, H., Hao, H. and Yang, H.Y. 2021. Oiling-Out Crystallization of Beta-Alanine on Solid Surfaces Controlled by Solvent Exchange. *Advanced Materials Interfaces.* **8**(2), p12.

Zihni, C., Balda, M.S. and Matter, K. 2014. Signalling at tight junctions during epithelial differentiation and microbial pathogenesis. *Journal of Cell Science* **127**(16), pp.3401-3413.

List of Abbreviations

AE	association efficiency
API	active pharmaceutical ingredients
Caco-2 cells	human colon adenocarcinoma cells
C_{CI}	capacitance
DLS	dynamic light scattering
F-actin	filamentous actin
FTIR	Fourier transform infrared spectroscopy
GI tract	gastrointestinal tract
HPLC	high performance liquid chromatography
MDCK cells	Madin-Darby Canine Kidney cells
MTT	3-(4,5-dimethylthiazol-2-yl)-2,5-diphenyltetrazolium bromide
NE(s)	nanoemulsion(s)
NP	nanoparticles
PBS	phosphate buffered saline
PE	Pickering emulsion
PDI	polydispersity index
ROA	routes of administration
SHU	Scoville heat units
TEER	transepithelial/transendothelial electrical resistance
TEM	transmission electron microscopy
TRPA1	transient receptor potential cation channel, subfamily A, member 1
TRPV1	transient receptor potential vanilloid 1
TRPV4	transient receptor potential vanilloid 4
WER	water ethanol ratio